Improving Brace Effectiveness for Adolescent Idiopathic Scoliosis Patients

Master thesis by
S. Wermink

Improving Brace Effectiveness for Adolescent Idiopathic Scoliosis Patients

by

S. Wermink

To obtain the degree of Master of Science

Department of Biomedical Engineering
Faculty of Mechanical, Maritime and Material Engineering
Delft University of Technology

To be defended on July 9th, 2019

Thesis Committee:
Prof. Dr. Ir. H. H. Weinans,   TU Delft, supervisor
Prof. Dr. Ir. H. Vallery   TU Delft
Dr. Ir. N. Tümer   TU Delft

TUDelft

ABSTRACT

Adolescent idiopathic scoliosis (AIS) is a three-dimensional deformity of the spine that can be treated by wearing a correctional rigid brace. The goal of brace treatment is prevention of curve progression, and in some cases the curve even decreases. The current problem concerning treatment of AIS lays in the design decisions made during manufacturing of the brace. Correctional forces are applied through static pressure pads added to the inside of the brace. Evaluation of the correct positioning and size of these forces is done through radiographic imaging which allows limited feedback intervals as cumulative exposure to ionizing radiation increases the risk of cancer development. The design of scoliotic braces is currently suboptimal as the manufacturing remains an inefficient process. Moreover, it was hypothesized that the corrective forces show decreasing time dependant behaviour due to viscoelastic properties of the human body adapting to the load.

The objectives of this study were therefore to increase the effectiveness of brace treatment, by determination of the time dependant behaviour and accurate positioning and sizing of correctional forces.

A dynamic brace was developed containing pressure regulated cuffs creating a three-point-bending system on the spine. A healthy (non-scoliotic) test subject wore the brace with the goal of creating a spinal curvature. The cuffs were tested on stress relaxation behaviour, which was needed to determine if possible changes in pressure were due to viscoelasticity of the cuffs or the body. The tests showed that pressure stayed constant over time, which excludes viscoelasticity of the cuffs. Moreover, compression tests were executed on a cuff to determine the relationship between external loads and internal pressures.

Ultrasound (US) imaging was used to evaluate the effect of the three-point-bending system on the spine. The images showed a curvature, but the results varied too much to draw conclusions from, as this imaging technique works best for large scoliotic curves. BoneMRI has higher imaging accuracy and adds an extra dimension, however supine positioning decreases the spinal curvature. The boneMRI results show a subtle curvature after applying pressure. The cuffs lengthened the spine and caused mechanical torsion. After one hour the lengthening remained equal but the mechanical torsion decreased to its starting value. Lengthening of the spine could be useful in brace treatment to create more space between vertebrae and facilitate vertebral realignment.

This research served as a proof of concept which can be further developed by testing on a scoliotic patient with a moderate spinal curvature. This could result in a dynamic brace used as a method to enhance the positioning and sizing of pressure pads for a static brace, or the dynamic brace design needs adjustment to use it as a daily worn brace which keeps correctional forces constant by adjusting pressures automatically.

TABLE OF CONTENTS

1

INTRODUCTION

1.1 SCOLIOSIS

Scoliosis is a 3-dimensional deformity of the spine, which includes a deviation in the coronal plane, changes in the sagittal curve, and an axial rotation of the vertebrae [1][2]. It can be categorized by three major etiopathogeneses - congenital, syndromic and idiopathic. Congenital scoliosis refers to innate abnormally formed vertebrae causing spinal deformities. Syndromic scoliosis is associated with a systemic disease. These are for example disorders of the neuromuscular system, skeletal system, connective tissue systems and neurofibromatosis [3]. Idiopathic scoliosis denotes a curve of unknown aetiology which can develop during different stages of life while growing. The underlying mechanisms of idiopathic scoliosis are poorly understood [4]. The three types, categorized depending on age onset, are infantile (0-3 years old), juvenile (4-9 years old) and adolescent (10 years old until closure of the growth plate [3]. Adolescent idiopathic scoliosis (AIS) is the most common type, affecting more girls than boys. This condition begins in early puberty and affects 1-4% of adolescents [4], while treatment is required for 0.3%-0.5% because of curve progression [5].

Cobb angle is a measure of quantitating scoliosis severity. It helps determine the curve progression, treatment type and the effectiveness of a certain treatment [6]. By help of a posteroanterior view of the spine, the superior and inferior end vertebrae are identified (figure 1). The angle between the proximal and distal ends of the vertebrae with the highest tilt are measured by drawing a line parallel to the upper endplate of the superior end vertebra, and parallel to the lower endplate of the inferior end vertebra. The perpendicular drawn lines form the Cobb angle (angle b) at their intersecting point.

Both skeletal and sexual immaturity influence the scoliosis curve progression negatively [7]–[10]. Age and gender are therefore important risk factors for the development of scoliosis. One speaks of curve progression when the Cobb angle is increased by 5 degrees or more, which is the smallest angular difference that can be measured accurately [11]. Moreover, the larger the curve at identification, the higher the chance of progression before [7] and after maturity [8]. Risser sign is an indication of skeletal maturity by measuring the degree of ossification of the pelvis to determine overall ossification development [12]. Grade 1 indicates 25% calcification, whereas the maximum grade of 5 indicates a full mature skeleton with 100% calcification and fusion of the ossified apophysis with the iliac wing.
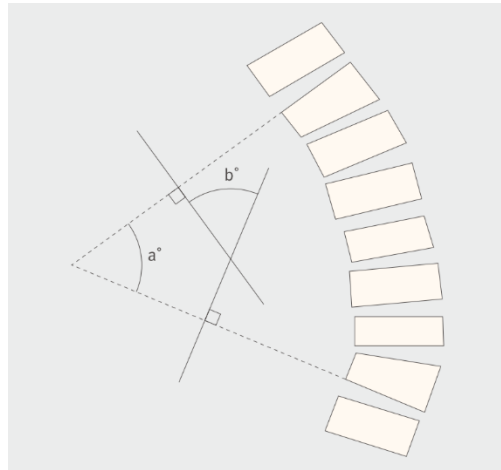
Figure 1: Determination of size of scoliosis curve by measuring Cobb angle [3][13]. *The lines drawn parallel to the to the highest tilted vertebrae create angle a. The perpendicular drawn lines form the Cobb angle (angle b) at their intersecting point.*

1.2 BRACING

Three types of scoliosis exist based on severity: mild, moderate and severe scoliosis, where patients have a deformity of maximally 20 degrees, between 20 and 40 degrees or above 40 degrees respectively (figure 2). The type of scoliosis is one of the most important determinants to select the best possible treatment option. Treatment options for AIS include observation to watch for progression, bracing or in severe cases surgery. Treatment, excluding observation, is always a severe burden as it consists of a rigid, constraining brace to be worn a great time of the day or an extensive surgical procedure that risks neurological damage [14].
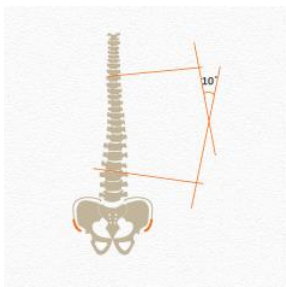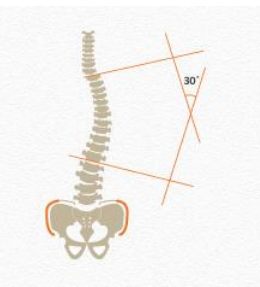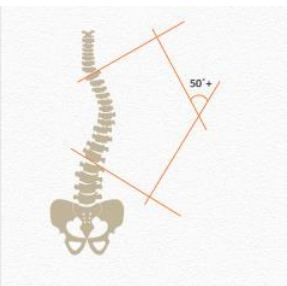

Scoliosis type	Mild	Moderate	Severe
Cobb angle	<20°	20°-40°	>40°
Treatment type	Observation	Bracing	Surgery

Figure 2: Relationship between scoliosis type and treatment [15]. *The Cobb angle indicates the severity of the disease which determines the treatment type.*

The goal of brace treatment is preventing curve progression by applying external forces to the spine. This treatment is therefore offered when patients contain a moderate Cobb angle and a low Risser stage (0-1), when halt of curve progression is still possible [3]. In some cases bracing does not only reduce progression, but also decreases the curve [16]. Weinstein et al. (2013) found a significant relationship between average hours of brace wear and the likelihood of successful treatment, where successful treatment was defined as a Cobb angle of less than 50 degrees while reaching skeletal maturity. Longer hours of brace wear were associated with a greater benefit [17]. An average wear of at least 12.9 hours a day is associated with a success rate of 90-93%.

Patient compliance with bracing prescription is described as the biggest challenge regarding non-operative management of AIS [17]. The goal of non-operative treatment is the prevention of curve progression, but in some cases the curve increases and surgical treatment is needed for correction and maintenance [18]. Surgery is considered when there is an indication of a Cobb angle greater than 40 degrees [17] because curves over 50 degrees tend to progress after maturity [19]. Surgery is needed for about 10% of scoliosis patients [9].

For a long time the effectiveness of bracing was questionable, but bracing has now proven to be successful in treatment of AIS [17]. Many review papers exist on comparing effectiveness of brace brand designs, which remains difficult due to inconsistencies in research protocols and disparity regarding the choice of outcome measures [20]. All brace designs have the same goal of preventing curve progression [21] by applying forces on the spine, but the way of implementation can differ. Braces aim to apply corrective forces on the spine by applying loads on the convex (outer) part of the curve and releasing loads on the concave (inner) part of the curve [22]. A three-point pressure system is created inside a brace to correct a C-shaped scoliotic curve. Opposite of the pressure point inside the brace, voids are created to provide room for the spine to move (figure 3) [23]. Wynarsky and Schultz (1991) suggested that there are two mechanisms that help to achieve correction of scoliosis: passive mechanisms such as external forces applied by brace pads and active mechanisms like muscle control to shift the trunk away from the pressure areas [24].
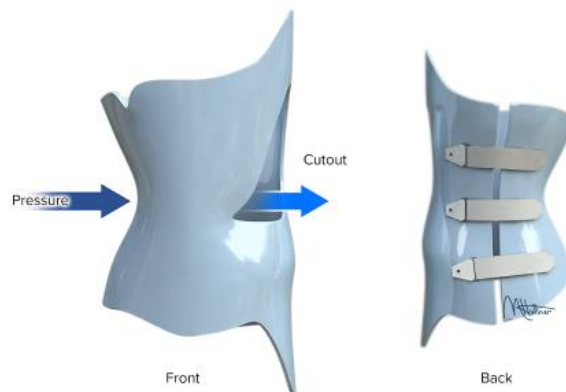

Figure 3: Working principle of a Boston brace [22]. *Opposite of every pressure point is a cut out, creating space for the body to realign. The brace material above and below the cut out create a three-point pressure system, together with the pressure point indicated with an arrow.*

Because of the 3-dimensional nature of scoliosis, corrections are needed in every anatomical plane. A brace provides detorsional forces by combining the three-point pressure system in coronal plane with pairs of forces in the transversal and sagittal plane. Pads designed with a specific shape, size and location are added on the inside of the brace to create pressure areas which cause derotational forces [25].

Implementation of the correctional forces is possible in different ways, therefore multiple brace designs have been developed over the years. An overview of existing brace concepts has been made based on manufacturing method (figure 4). A complete overview of the most important advantages and disadvantages per development method is visualized in Appendix I. An image of the most often used brace brands is shown per category. Braces can be vacuum formed, 3D printed or are prefabricated. A positive trunk model is used as a base for vacuum forming of the brace. This can be obtained by creating a plaster cast over the patient's body, or by milling/carving of a foam block with help of computer aided design and computer aided manufacturing (CAD/CAM) and additionally finite

element modelling (FEM) [21], [26], [27]. Pressure pads and brace openings can be added to create a three-point pressure system. The biggest advantage of vacuum formed braces is the personalized fit.

A distinction can be made between prefabricated rigid braces and soft braces [21]. The most common used brace worldwide is the Boston brace module. Different shapes and sizes of the brace are readily available and only hand measuring of the patient's geometry is needed. Pressure pads are added and material is removed to personalize the brace. Controversy remains regarding the effectiveness of soft braces for moderate scoliotic curves [28], [29]. Prefabricated braces are fast available which makes them attractive, however the fit is not as optimal as vacuum formed or 3D printed braces.

Finally, there is one 3D printed brace available on the market, which is the UNYQ brace [30]–[32]. The benefits of a 3D printed brace are creating a lighter, higher ventilated and more comfortable brace by adapting wall thickness and including local textures.

Vacuum forming			Prefabricated		3D printing
Plaster cast	CAD/CAM	CAD/CAM + FEM	Rigid brace	Soft brace	
Wilmington brace [26]	Lyon ART brace [26]	Research trial brace [33]	Boston brace module [21]	SpinceCor brace [21]	UNYQ brace [31]

Figure 4: Overview of brace concepts categorized by development method.

For all braces holds that skill and experience of the orthotist are the major factors which affect the design of the brace and no real time feedback is available to determine the optimal pad location which makes it a subjective process [34].

1.3 IMAGING

X-ray imaging in the treatment of scoliosis is needed to diagnose, analyse the effect of treatment and watch for progression of the deformity [35]. Traditionally anterior-posterior and lateral upright images are taken, more recently standing low-dose biplanar radiography became available which can be used for three-dimensional reconstructions to get better understanding of the true three-dimensional deformation of the spine [36].

No standard protocol for the timing of taking radiographic images exists. Some physicians routinely take in brace X-rays at the day of orthosis fitting. Others suggest taking it after wearing the brace for two to four weeks, to allow for viscoelastic changes in the body because of correctional forces. Subsequent X-rays are needed to analyse the bracing effect for a minimum of two years, these can be taken at three to twelve months intervals, depending on the healthcare institution protocol [37]. Follow-up images might be taken regularly regardless of a patient's age, curve magnitude, risk for progression, while consciously creating personalized protocols in order to minimize radiation exposure is preferred. Some physicians take in brace X-rays, others take out of brace X-rays, while some take both on one day [38]. This cumulative amount of ionizing radiation can be dangerous in the development of cancer. A long-term follow-up study executed on the Danish population, revealed that adolescent idiopathic scoliosis patients have a 5 times higher risk on developing cancer compared to the normal Danish population. Endometrial and breast cancer had the highest incidence. An average of 16 radiographs were taken during treatment, which may result in relatively high cumulative radiation doses. There is no radiation free method currently available or being used to accurately evaluate scoliosis [39].

Radiation free imaging techniques to visualize the spine involve magnetic resonance imaging (MRI) and ultrasound techniques. MRI does not visualize cortical bone very well, it is expensive, time consuming and not performed upright. Due to gravitational forces the geometry of the body changes. However, it delivers a three-dimensional image which is preferred in order to visualize the three-dimensional character of the scoliotic spine. Another method to visualize the scoliotic curve without exposure to radiation is the use of ultrasound. Ultrasound images can be taken in upright position and are faster and more pleasant to take. However, the person taking the images needs to be very skilled [35]. Since the use of ultrasound technology, it is possible to detect a coronal angle by spinous processes (SP) and transverse processes (TP) which can be seen in figure 5 and 6 [40]. Brink (2018) discovered that ultrasound angles were 15%-37% smaller compared to radiographic Cobb angles. However, linear correlations were found between all ultrasound angles and the Cobb angle.

Determination of the optimal location of pressure pads is not easy in the fitting process of the brace. Radiographs taken at pre-brace stage do not provide real time information of the spinal deformity and the curvature changes after application of pressure pads. This makes the current way of brace development a very inefficient and ineffective process.

Another factor which decreases brace effectiveness is the force reduction of the pressure pad areas due to the viscoelastic behaviour of the body and the realignment of the spine [41]. A static force is applied to correct for spinal deformities, when this load continues to work after initial correction there is creep behaviour occurring over time [42]. Creep behaviour is highly depending on the stiffness of the spine. In the article of Lou (2012) the forces of major pressure pad areas decreased continuously after two months of wearing the brace which is due to viscoelastic changes of the human tissue.

Inspiration is obtained by the use of the Ponseti method [43] which treats clubfoot patients by gently manipulating the position of the foot towards a physiological position by using cast. The foot first resists against the new position by pressing against the cast, but over time it will adapt and the forces decrease. A study by Giesberts et al. (2018) showed that forces halved within an hour which suggests adaptation of the foot. It is therefore expected that the spine quickly adjusts to the brace which decreases forces. If this is the case, effectiveness can be improved by decreasing the interval between brace adjustment or creating a dynamic brace which keeps forces constant.

1.4 OBJECTIVES

This study aims to develop a method to improve the effectiveness of brace manufacturing concerning the design of pressure pad locations and size, and decrease the exposure to ionizing radiation of adolescent idiopathic scoliosis patients. An additional aim of this study is to test the hypothesis of decreasing brace forces over time due to adjustment of the body, if this is the case correctional effectiveness could be gained by keeping brace forces acting on the body constant over time.
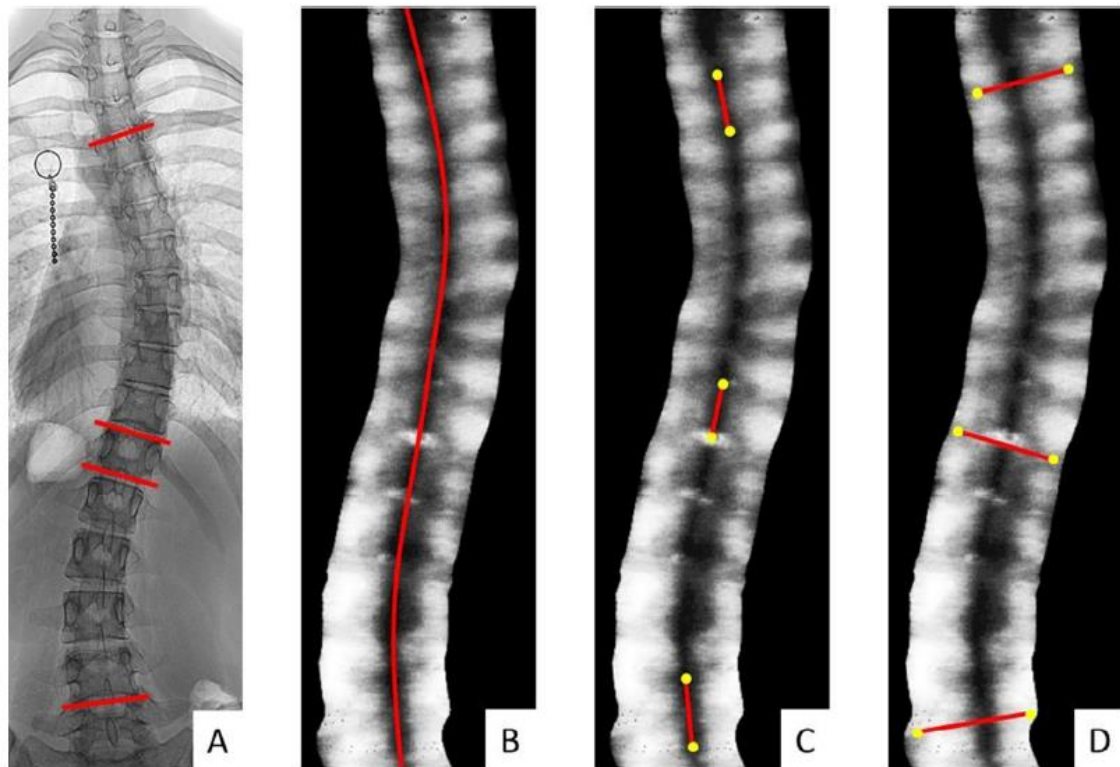
Figure 5: All images show spinal angles of the same patient. Image A shows the coronal Cobb angle measured on a radiograph. B shows automatic obtained SP angle by Scolioscan software. Both C and D show manually obtained spinal angles by SP and TP respectively. The angle between the red lines of the most tilted vertebrae were measured [35].

Figure 6: The bony features of the vertebral column [44]*. The landmarks used for ultrasound imaging are the spinous and transverse processes.*

2

MATERIALS AND METHODS

2.1 BRACE DESIGN

A way of improving brace development is by enhancing the way pressure pad locations are chosen without ionizing radiation exposure. A dynamic test brace was developed where inflatable pressure regulated pads are added on the inside of the brace, attached by Velcro to provide for location changes (figure 7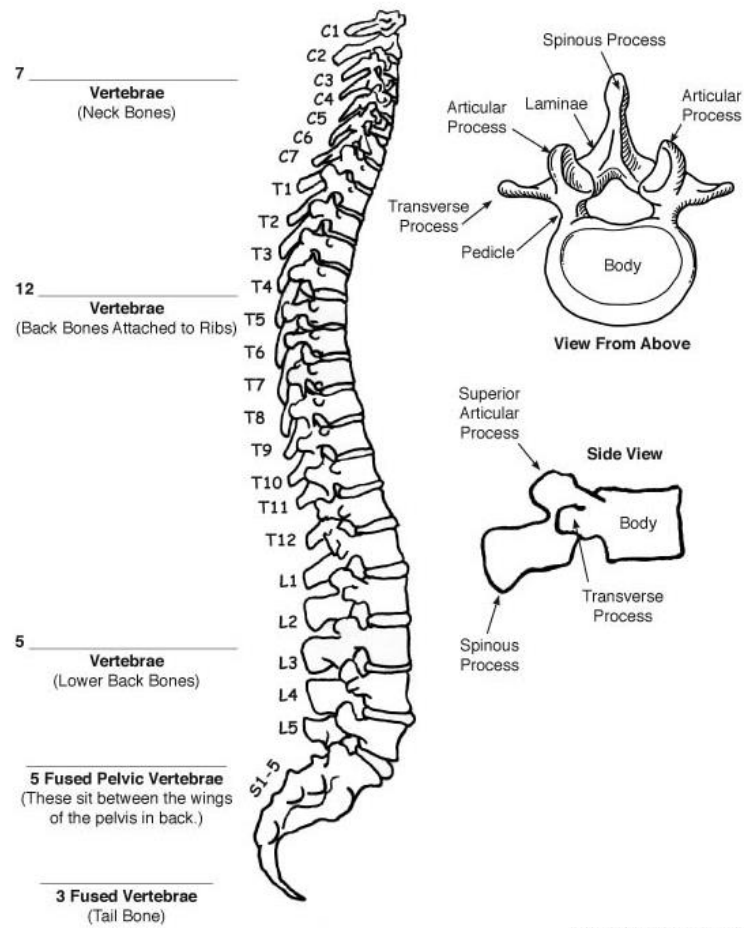). As this method purely serves as a proof of concept, this test brace was designed for a healthy twenty-four years old female subject (not suffering from scoliosis). This means that by wearing the brace, the goal is to create spinal curvature in an initial straight spine (figure 8).

Anterior   Posterior   Lateral

Figure 7: Dynamic Neofrakt brace design, showing the air cuff locations on the anterior and posterior view. When taking ultrasound images, a part of the back side of the brace can be removed. The maximum dimensions are given in mm.

The brace was made in the plaster room of the University Medical Center in Utrecht. This corset is commonly used as conservative treatment method to solve spinal problems and minimizes the possible bending, turning and stretching forces on the vertebrae. For this research the test subject first surrounded her body with a 30 mm thick polyether foam and wore a cotton shirt over it. This cotton shirt is double layered and serves as a case to pour liquid polyurethane in. After hardening of the polyurethane, some trimming was needed to increase comfort and freedom of movement.

The backside of the brace is partly open to create room for an ultrasound probe to make skin contact. Between the brace and subjects' body three inflatable and pressure regulated cuffs were placed to

recreate a three-point pressure system. The brace is overall 30 mm oversized, this extra space serves as room for the inflatable pressure cuffs to create a true three-point pressure system which means that the subjects' body only has contact with the pressure cuffs and no skin to brace contact is present when standing. The Karl-Hanz aneroid blood pressure cuff upper arm model was used as pressure regulated air cuffs, with a maximum pressure of 300 mmHg (figure 9). It consists of a rubber cuff with two tubes connecting to a gauge to read the pressure and a bulb with release valve to adjust the pressure. The cuff is enclosed by a textile case.

This dynamic test brace can be used as an aid in the development stage of a proper daily worn brace, to determine the optimal pad pressure, location and size while using ultrasound imaging.
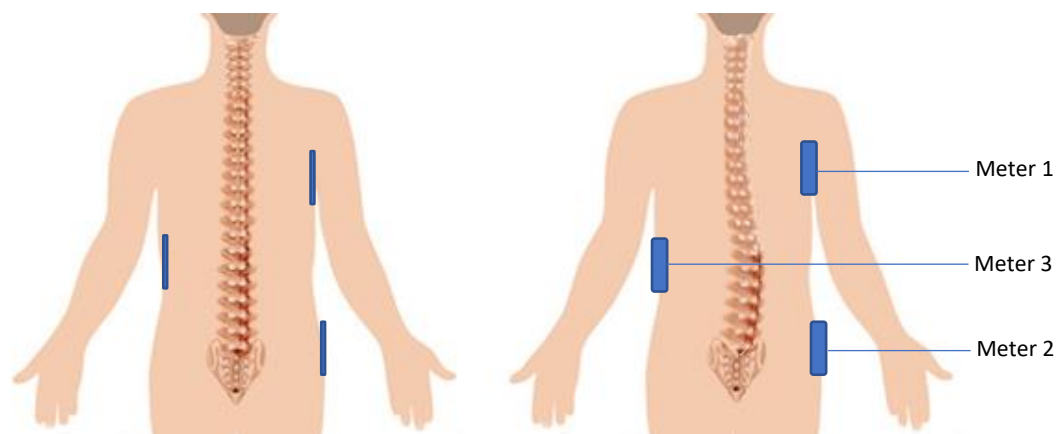
Figure 8: Visualization of the spinal deformity created by the test brace. The left image shows the positioning of the deflated cuffs, the right image shows inflated cuffs and the expected spinal effect. Adjusted image from Boulder, neurosurgical and spine associates [45]*.*

Figure 9: Karl-Hanz aneroid blood pressure cuff upper arm model. The rubber cuff connects to a gauge to read the pressure and a bulb with release valve to adjust the pressure. The cuff is enclosed by a textile case (detached on this picture) with Velcro to make attachment to the brace possible. The uninflated dimensions of the cuff are 145x230 mm.

2.2 STRESS RELAXATION MEASUREMENTS

A total of six blood pressure cuffs were tested on stress relaxation behaviour. This is needed in order to interpret the pressure values of the blood pressure cuffs accurately. Vis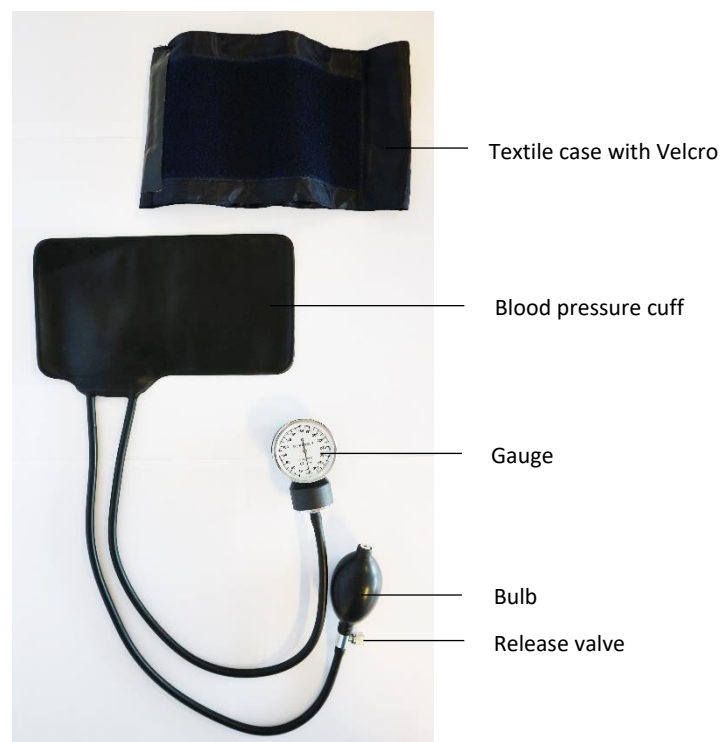coelastic materials show stress relaxation behaviour, which is a time-dependent decrease in stress under a constant applied strain. This test determines whether changes of pressure values over time are due to viscoelastic changes of the body, or a loss of force in the blood pressure cuffs due to stress relaxation when wearing the brace, or both.

Moreover, the goal of this test was to analyse if all blood pressure cuffs showed the same mechanical behaviour. If not, it is important to determine which three blood pressure cuffs are most suited to use in the ultrasound and MRI tests.

In order to minimize the possible viscoelastic behaviour of the blood pressure cuffs, the textile case was not removed. This case only covers the rubber cuff and not the tubes, which might also show some viscoelastic behaviour.

The blood pressure cuffs were confined on two sides with rigid wooden boards which have 30 mm between them to mimic the brace-body distance (figure 10). The blood pressure cuffs were inflated to an initial pressure and a camera (EOS M10, Canon) created a time lapse to keep track of the possible pressure changes over time. Confining the cuffs created a constant state of strain.

A total of six tests were performed. Initial pressure values of 150 mmHg and 200 mmHg were chosen for all six blood pressure cuffs. All tests took at least two hours and were repeated three times to validate the results. At least one hour of waiting was calculated between execution of experiments, to avoid the effect of starting an experiment with pre-stretched material.
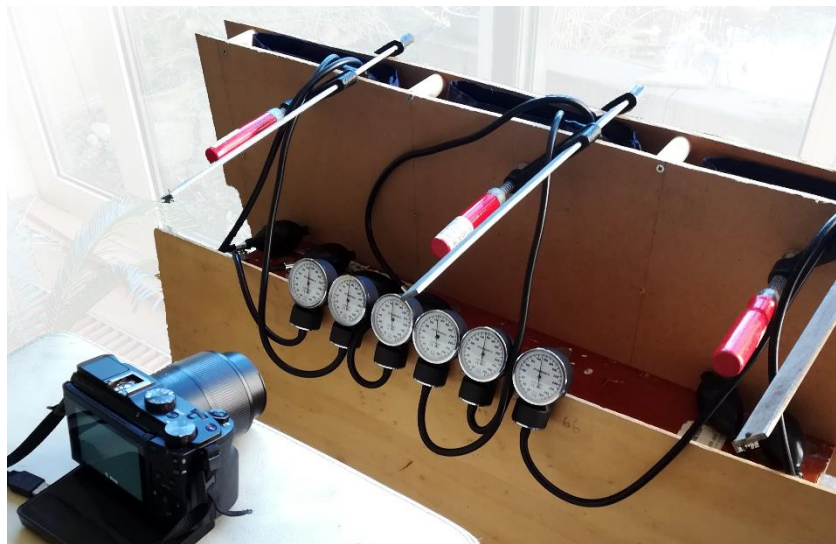

Figure 10: Stress relaxation test setup. A total of six blood pressure cuffs were positioned between two rigid wooden plates. Possible changes in pressure were tracked by filming the pressure meters.

2.3 COMPRESSION TESTS

In order to get a better understanding of possible outcomes of a qualitative brace research, fundamental research into the relationship of the pressure inside the cuff and exerted forces onto the body is needed. The aim of doing compression tests is therefore to be able to determine what forces are applied on the body for specific pressures. This will give better understanding of the stiffness of the spine.

The relationship between force and pressure can be explained by equation 1.

$$P = \frac{F}{A}$$

Eq. 1

Pressure (P) is the amount of force (F) applied at right angles to the surface of an object per unit area (A). This is expressed in Pascal (Pa) which is equal to Newton (N) per square meter (m^2).

Compression tests on blood pressure cuffs have been executed to determine whether there is a relationship between pressure, load, and displacement. Different test setups were created that mimic the behaviour of the cuff when placed between the body and brace, an overview of all possible setups can be found in Appendix II.

The most important setup is explained in figure 11, which is setup A from Appendix 1. The test starts by determining the initial displacements (d_i) while the blood pressure cuff is still deflated. The second step is to inflate the blood pressure cuff until a certain initial predefined pressures (P_i) is reached. The compression machine then starts to decrease the distance between the load cells with a speed of 3 mm/min. The change in distance is defined by Δd. A load cell with a maximum of 5 KN is used. Changes in internal pressure were tracked by filming (EOS M10, Canon) the values of the gauge meters.

This test was executed for three different d_i values and five different P_i values of the blood pressure cuff. The initial displacements were chosen to be 20, 30 and 40 mm which is assumed to be equal to the distance between the body and the brace. The initial pressures were chosen to be 50, 75, 100, 125 and 150 mmHg. Higher initial pressures were not needed as the pressure rises with increasing Δd. All tests were executed with the same blood pressure cuff and manually stopped at the maximum pressure (P_{max}) of 250 mmHg.

Setup B and C from Appendix II had an infinite initial displacement, this means that at t = 0 the blood pressure cuff is inflated to a certain pressure and the load cell does not touch the cuff. The load cell is then lowered with a speed of 15 mm/min until a maximum pressure of 200 mmHg is reached inside the cuff. Setup B was executed five times, with the same initial pressure values as setup A. Setup C mimics the brace-body situation by including three blood pressure cuffs, all initially inflated to 100 mmHg, the maximum achieved pressure was 250 mmHg.
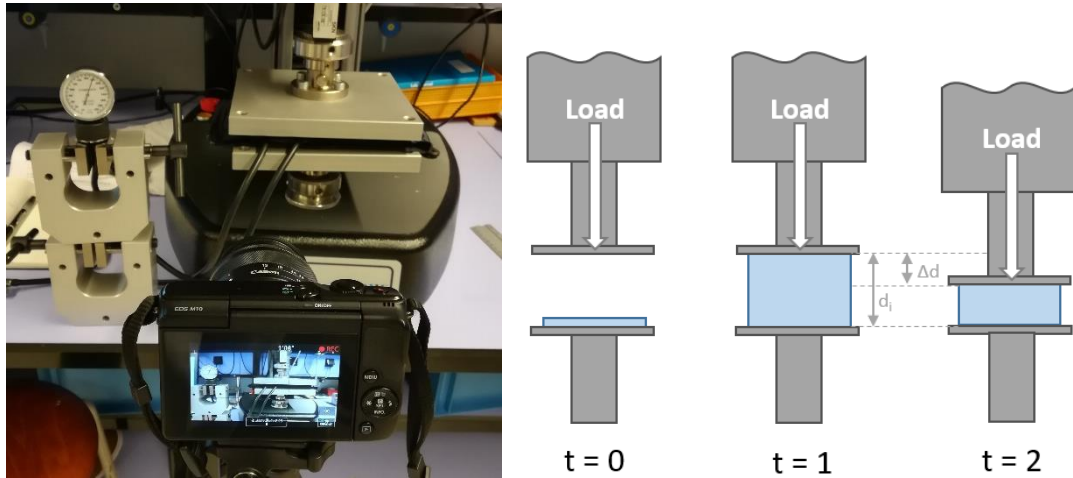
Figure 11: Compression test setups. Left: image of the complete test setup, the camera keeps track of pressure differences in the blood pressure cuff while the load cell is moving down. Right: schematic overview of the compression test. At t=0 the initial displacement (d_i) is determined, the pressure (P) is still 0. At t=1 the initial pressure (P_i) is implemented without changing d_i. At t=2 the d_i decreases with a speed of 3 mm/min.

2.4 ULTRASOUND TEST

The aim of this study is to discover a relationship between applied pressure and spinal curvature using ultrasound imaging, and to test whether this relationship is time dependant. Only two-dimensional imaging is possible with ultrasound which will likely show a curvature, as most deformation is expected in coronal plane.

Imaging of the spine was accomplished by using the Scolioscan system (Model SCN801; Telefield Medical Imaging Ltd, Hong Kong). Freehand scanning using the linear ultrasound probe (center frequency of 7.5 MHz, width of 75 mm), combined with a sensor to detect the position and the orientation of the probe created a 3-dimensional image of the spine. The final two-dimensional coronal result was based on the 3D reconstruction [35], [46]. As the ultrasound probe needs skin contact in order to create an image, the mid part of the back side of the brace was removed. Scanning was executed according to three steps visualized in figure 12. The lower strap of the brace remained fixed at all times because the ultrasound probe started measuring just above the lowest strap. After moving the probe continuously up to the upper strap, the mid strap needed to be fixed while remaining skin contact. After fixation of the mid strap, the upper strap could be detached so the probe could be moved upwards to finalize the ultrasound image.

Figure 12: Sequence of strap attachment and detachment during ultrasound scanning in order to preserve brace stiffness.

Three different tests were executed while the test subject was wearing the brace. For the first test the influence of increasing pressure on the spinal curve was tested. A total of four scans were made, the first one in neutral position while the subject was wearing the brace without inflation of the blood pressure cuffs. The second scan was made after increasing the pressure in all cuffs to 100 mmHg, the following two scans were obtained after increasing the pressure in all cuff with 50 mmHg respectively. When increasing the pressure, attention should be paid on simultaneous inflation of all blood pressure cuffs to prevent the brace from moving towards one side of the body.

Another aim of this study is to test the hypothesis of decreasing brace forces over time due to adjustment of the body. Time dependant behaviour of the spinal curve can be tested by keeping the amount of air in the blood pressure cuffs fixed and measure the possible change of pressure within the cuffs and the effect it has on the spinal curve.

For the second test, the test subject wore the brace for two hours while sitting or standing. A neutral scan was first obtained where the subject wore the brace without inflating the blood pressure cuffs. The cuffs were inflated until 100 mmHg each and a second scan was made. The test subject continued wearing the brace for two hours while standing or sitting. One-hour time intervals were chosen as third and fourth scan. While the subject was wearing the brace, the pressure values were written down in time intervals of 10 minutes to capture possible changes. To validate the tests on similarity, every scan was repeated once. It took on average 5 minutes to walk to the Scolioscan, make two in-brace spinal echo's and walk back. The patient was standing while taking the ultrasound images, and sat in another room while waiting for the next scan, wearing the brace at all times.

A maximum pressure of 100 mmHg was chosen because this value is comparable with maximum values used in literature. In the study of Wong (2000), the mean pressure of the pressure pads was found the be 53.2±13.3 mmHg [47]. Chalmers (2012) developed a dynamic brace which regulates pressure to keep forces constant while breathing and changing posture. A target pressure of 40 mmHg was being chosen [48]. A study of Lou (2005) measured the average pad pressure in braces while wearing them for four weeks which was 58±20 mmHg [49] and stated that a maximum pad pressure of 120 mmHg could be achieved on the body [50]. Finally a study of Perie (2013) explained that pressures of 70 mmHg were measured in the Milwaukee brace, and pressures over 30 mmHg were measured in the Boston brace [51].

This same test was executed with a pressure of 200 mmHg in all blood pressure cuffs in the hope to create larger spinal curvature. The complete overview of all ultrasound test can be seen in Appendix III.

To analyse the ultrasound images, the Scolioscan software automatically measures spinal processes (SP) and computes a spinal curve value. The automatic SP angle is based on the extraction of bony features from volume projection imaging [46]. The SP and TP (transverse processes) angles cannot be compared to radiographic Cobb angles as they underestimate the Cobb angle. However, they can be compared between themselves which makes it a relevant measuring technique.

2.5 MRI TEST

The aim of this MRI study is to accurately measure the changes in spine orientation when applying pressure and to analyse possible time-dependant behaviour of the spine. These scans were additionally needed on top of the ultrasound scans to provide information about the possible axial and sagittal deformation. The brace pressures are applied in coronal plane but this does not necessarily mean that is causes a purely coronal deformation. Looking at the 3-dimensional deformity gives more insights, because scoliosis is originally a complex 3-dimensional deformity. Moreover, this measuring technique is more accurate than ultrasound and gives a clearer reconstruction of the spine.

In order to make the brace MRI compatible and safe, adjustments were necessary.
- Foam was added to the inner backside of the brace, to keep the body centrally located. This is the same 30 mm thick polyether foam as was used to create the oversized brace. On blood pressure cuff locations, foam was removed.
- All magnetic parts were removed both on the brace itself as on the gauge of the blood pressure cuff.
- The six rubber tubes belonging to three different blood pressure cuffs were elongated by a 3-meter-long PVC transparent tube. Coupling pieces were used to connect the different tubes. The elongated tubes were needed to keep the pump and gauge further away from the MRI, because they contained metallic parts.
- Clips were used to block the air passage between the gauge and the rubber cuff, and between the bulb and the rubber cuff. So that the gauge and cuff could be removed after usage, while keeping the pressure constant.

A total of three tests were made. Starting with a neutral MRI, which includes wearing the brace without inflation of the cuffs which functions as control image. After finishing this measurement, all cuffs were inflated to 100 mmHg and the next measurement was made. One hour later another MRI was taken, without altering the air inside the blood pressure cuffs.

The test subject has to lay still and cannot move position at all times during this experiment to make comparison between images more convenient (figure 13). The brace was therefore already worn during the neutral imaging, with the uninflated blood pressure cuffs being positioned correctly. The gauge and pump were not yet attached, because it is preferred to keep them outside the MR room when executing the tests. After finishing the first MRI, the gauges and pumps were attached to the extension tubes. Pressure inside the cuffs was increased simultaneously by two researchers to 100 mmHg. After reaching the correct pressures, the tubes were clamped and the gauges and pumps were removed for the next MRI to be taken. In order to watch for time influenced changes in the spine, a full hour was waited before execution of the next MRI.

It was not possible to watch for changes in pressure, because of the removal of the gauges. It was therefore needed to execute an extra experiment outside of the MR with the same setup to check for possible changes in pressure. The test subject was wearing the brace while laying down with all blood pressure cuffs inflated to 100 mmHg. Every 10 minutes the pressure values were written down up to a maximum of 60 minutes.

Figure 13: MRI test setup. The test subject is wearing the brace with inflated blood pressure cuffs. The tubes of the cuff are clamped, to prevent loss of air. The transparent tubes are used to inflate the cuff from a distance, but the gauge and pump were removed after attachment of the clamps.

This experiment was executed in a clinical scanner with a magnetic strength of 1.5 Tesla. This relatively low magnetic strength was chosen because of the reduced chance of artefacts. MRI is typically used for soft tissue contrasts, but in this case interest lays in imaging of the bone. A special software solution which uses deep learning to recognize bone tissue on MRI's was used to create a CT-like image. This method is called BoneMRI, and it complements the soft tissue images.

Adaptations were made to the study of Schlösser (2014) to analyse the spinal deformations in three dimensions [52]. Semi automatically in-house-developed software was used (ScoliosisAnalysis, Image Sciences Institute, Utrecht, the Netherlands) to measure mechanical torsion, as well as the anterior-posterior and right-left symmetry of each individual vertebra and disc between T2 and L5. Transverse sections were reconstructed of all endplates of each vertebrae (figure 14). Semi-automatic calculations were executed taking rotation and tilt into account. Torsion was calculated by measuring the degree of axial rotation between superior and inferior endplates. Asymmetry was calculated by measuring the intervertebral disc and vertebral body height, comparing anterior-posterior and left-right symmetry (figure 15). All measurements were executed twice and averaged out, to minimize the effect of possible outliers.
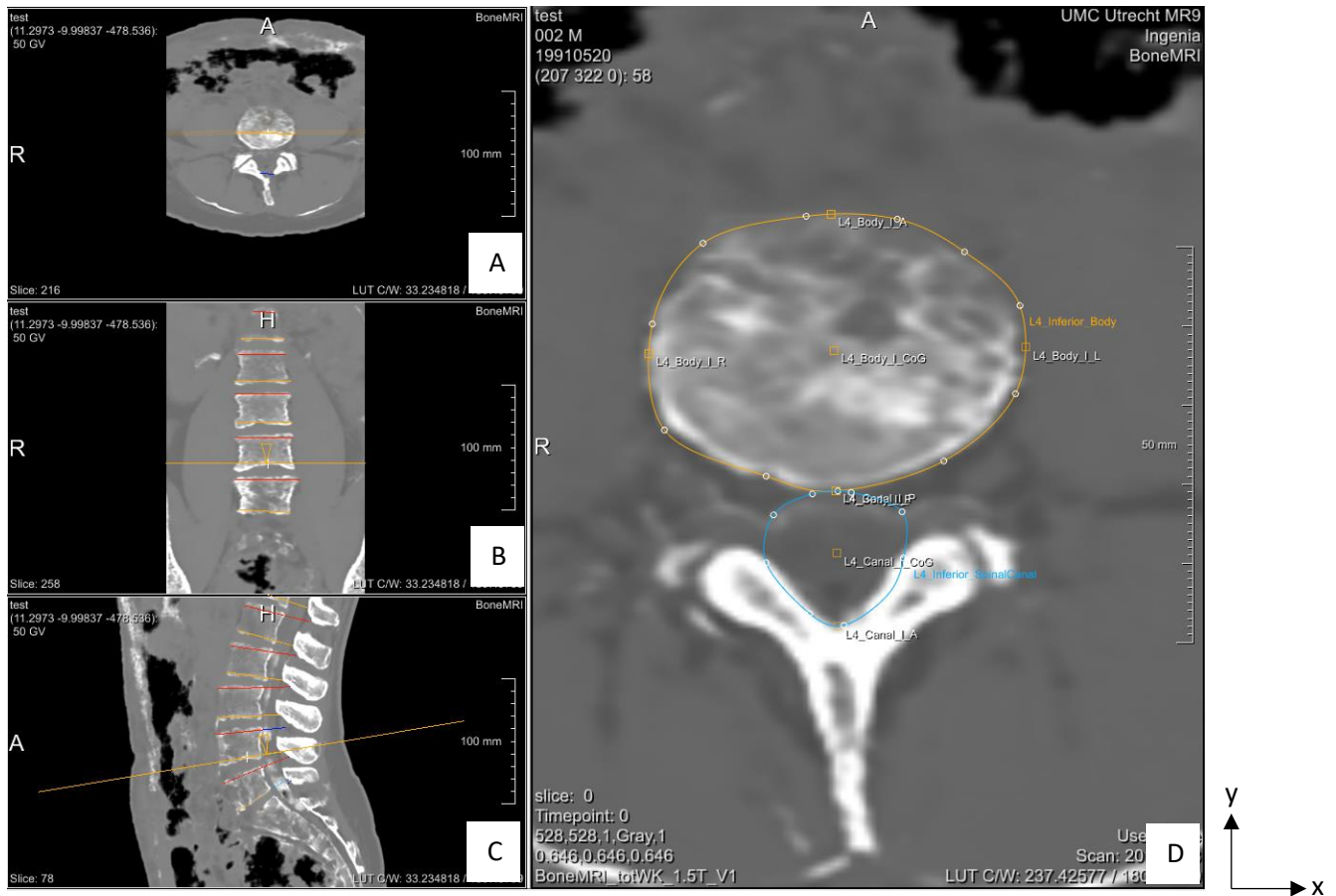
Figure 14: ScoliosisAnalysis software layout. A and D show the transverse plane, B coronal plane and C the sagittal plane. The position and orientation of each superior and inferior endplate was manually defined. The software automatically calculated the anterior-posterior axis and the right-left axis. The coordinates of the most anterior, posterior, left and right positions of the endplates was calculated. The exact distance between the coordinates of two adjacent endplates defined the height of the vertebral bodies and disc.
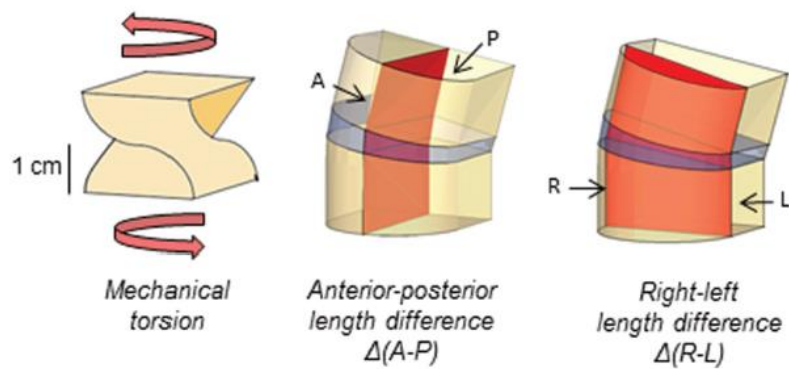

Figure 15: Schematic illustration of measured parameters from Schlösser (2014). The letters A, P, R and L represent anterior, posterior, right and left respectively. Mechanical torsion is defined by the difference in axial rotation between the superior and inferior endplate. Anterior-posterior and right-left length differences were measured in the true sagittal and coronal plane respectively.

3

RESULTS

3.1 STRESS RELAXATION MEASUREMENTS

A total of six experiments were executed. Initial pressure values of 150 mmHg and 200 mmHg were chosen for all six blood pressure cuffs. All tests took at least two hours and were repeated three times to validate the results. Graphs of the measurements were only visualized for a maximum of two hours, as this is only relevant for the ultrasound and MRI test. Appendix IV shows an overview of all executed tests.

Meter 1, 2 and 4 show the most constant and least decreasing pressure values and were therefore used for brace testing. These meters do not show significant decreases in pressure and viscoelastic behaviour is therefore excluded in the cuff. The minor decrease could be caused by a leakage or viscoelastic behaviour of the tubes. There was a higher decrease in pressure for the 200 mmHg test.

3.2 COMPRESSION TESTS

A total of three compression test setups were used, all carried out five times for different initial pressure (P_i) values of the blood pressure cuff. Figure 16-18 show the results for the initial displacement of 20, 30 and 40 mm respectively.

The solid lines show the results of the experiments for different P_i values. These pressure values within the blood pressure cuff change due to a change in displacement. The blue dashed lines indicate the internal pressures. A trend was discovered for the blue lines which shows that every specific internal pressure value together with a certain displacement, corresponds to a specific load value. Comparing figure 16-18 shows that for a smaller initial distance, higher loads can be achieved with the same starting pressure. Hence, it is possible to relate an internal pressure in the blood pressure cuff to a force range, when knowing the distance of the space the blood pressure cuff is enclosed in. Finding this out was the goal for the compression tests.

Figure 19 shows a graph combining the compression tests results, excluding the compression test with an initial displacement of 30 mm. A linear model was developed to describe the relationship between the brace-body distance and applied load, for different pressures. The formula describing this relationship is given for P = 100 mmHg, calculated via linear regression analysis (Excel, Office 2019) (equation 2). The equations for all pressures are given in Appendix VI. L (load) is a function of d (distance) for a specific pressure value. These values are only valid for a distance between 20 and 40 mm, as the load is expected to increase exponentially after decreasing more than 20 mm.

$$L_{P=100}(d) = -6.5 \cdot d + 372 \qquad\qquad \textit{Eq. 2}$$

The graph including the initial displacement of 30 mm shows non-linear behaviour (Appendix VII). The distance between the load cells together with a specific internal pressure indicate what force is generated. The higher loads are caused by smaller distances, because the blood pressure cuff is pressed down which increases the contact area. The lower internal pressure lines look smoother due to less data points being available. Figure 19 could be used as an estimation of forces acting on the body for a specific pressure and distance between the body and brace.

In figure 17 the line which shows the values of Pi = 50 mmHg is excluded from the graph. The line showed atypical behaviour comparing to the other results in the graph. This is due to a mistake when saving the values of the compression test, because the correct values were overwritten. In order to prevent confusion, this line is left out. Moreover, it does not provide additional needed information and therefore this experiment is not repeated.

Appendix V shows the results of the extra executed compression tests. The maximum internal pressure values achieved for setup C were $P1_{max}$ = 250 mmHg, $P2_{max}$ = 164 mmHg and $P3_{max}$ = 178 mmHg.

Figure 16: Blood pressure cuff compression test results of an initial displacement of 20 mm, showing five measurements. The solid lines indicate the five measurements with different initial pressure values (Pᵢ). The blue dashed lines indicate the relationship of the internal pressure in the blood pressure cuff with regard to the applied load.
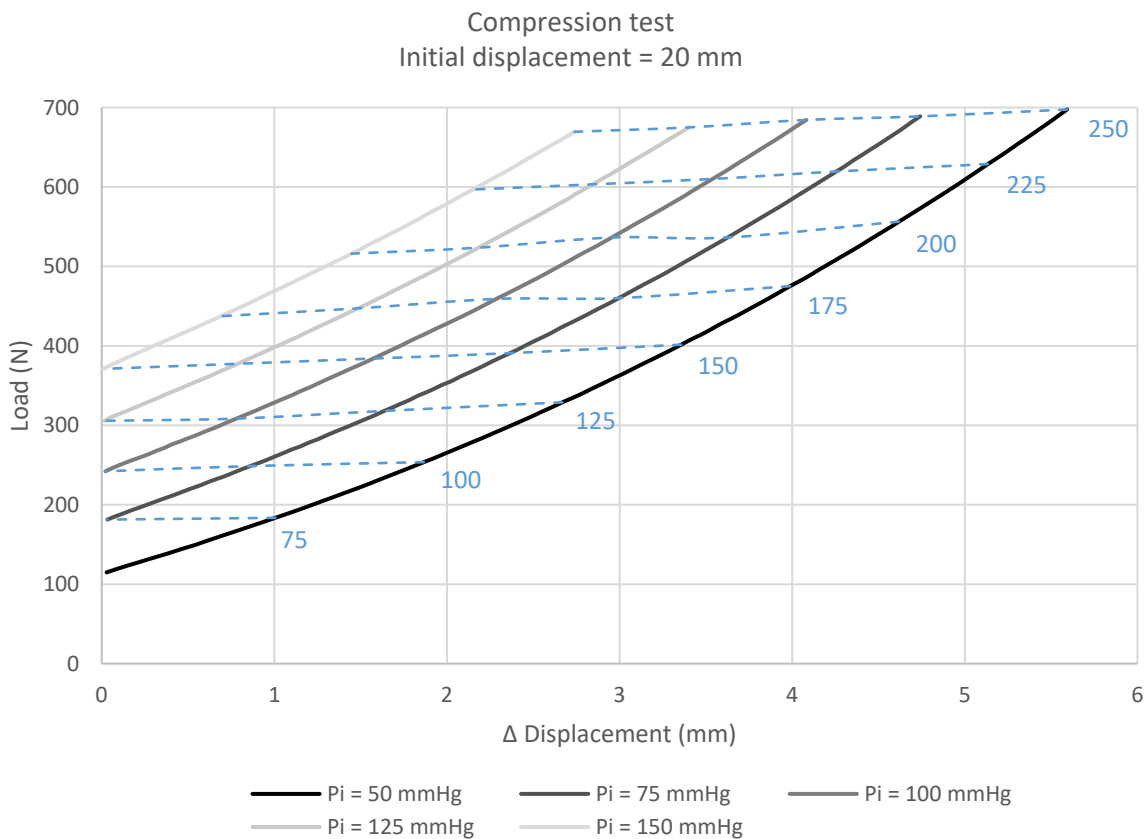
Figure 17: Blood pressure cuff compression test results of an initial displacement of 30 mm, showing five measurements. The solid lines indicate the five measurements with different initial pressure values (P_i). The blue dashed lines indicate the relationship of the internal pressure in the blood pressure cuff with regard to the applied load.
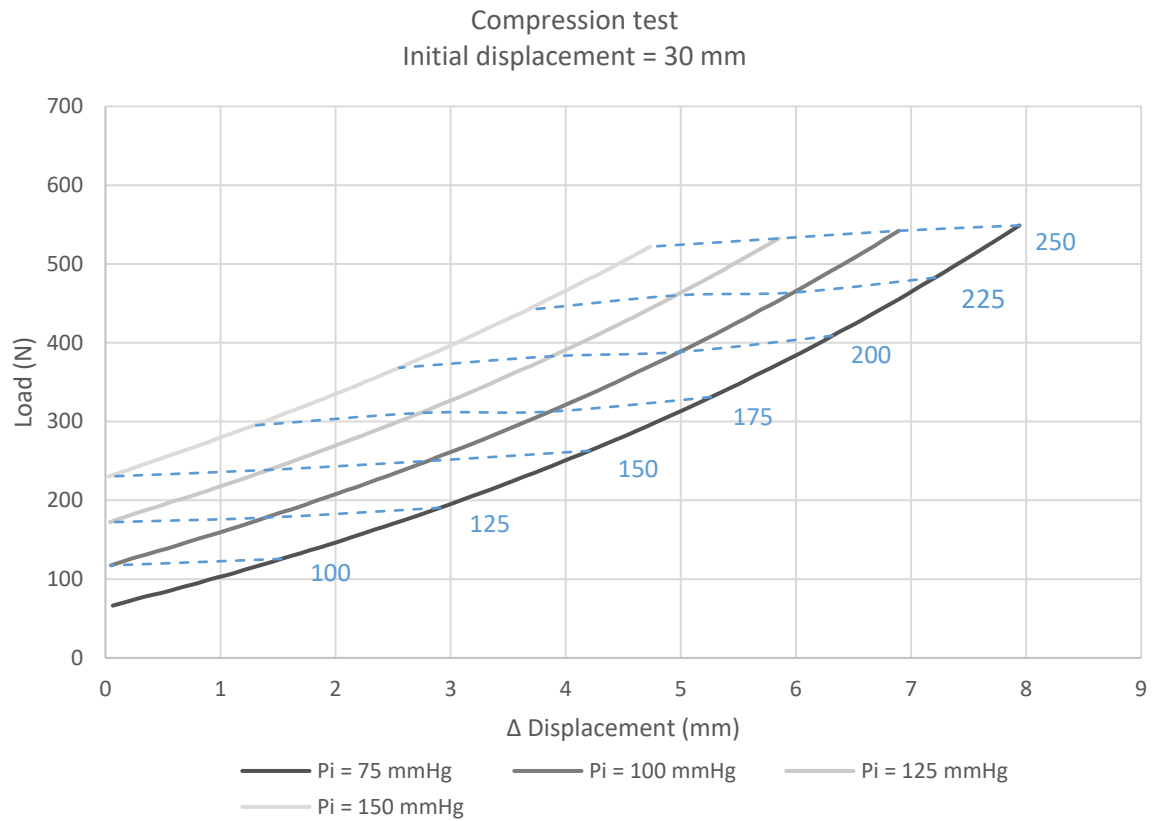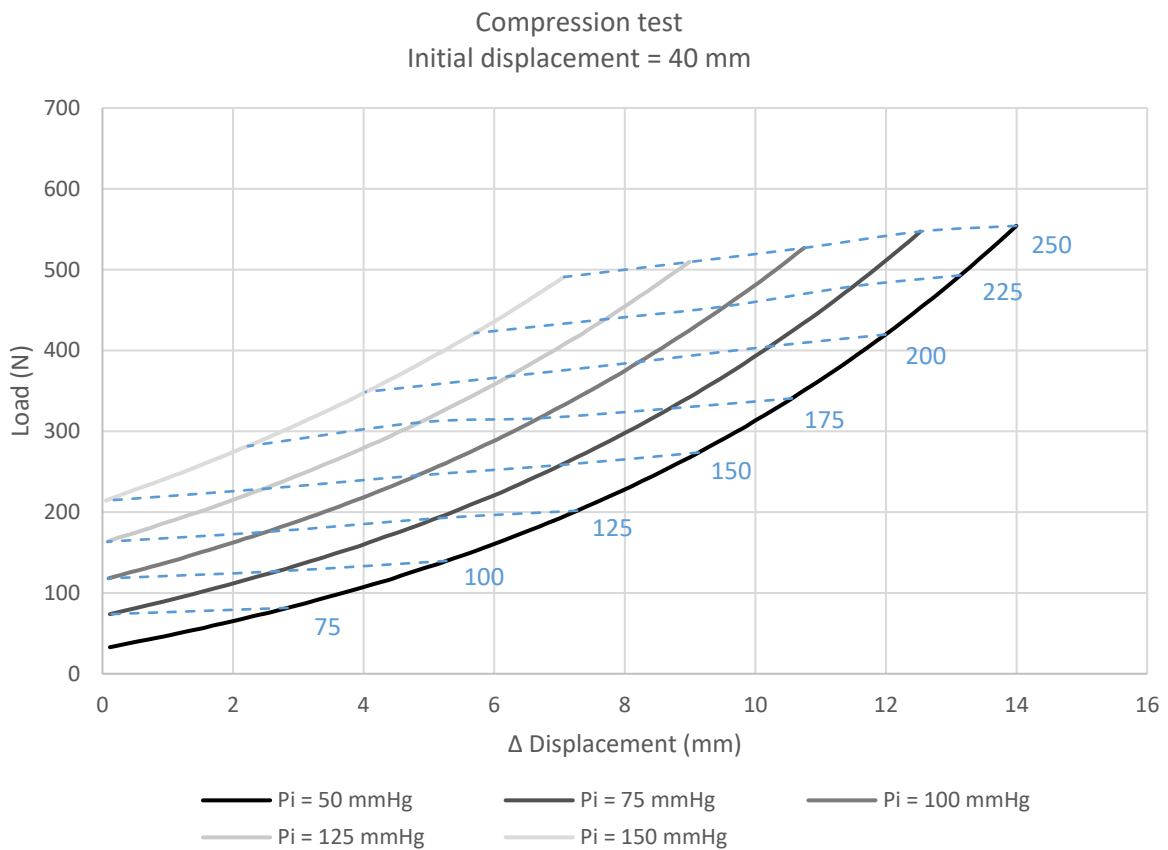

Figure 18: Blood pressure cuff compression test results of an initial displacement of 40 mm, showing five measurements. The solid lines indicate the five measurements with different initial pressure values (P_i). The blue dashed lines indicate the relationship of the internal pressure in the blood pressure cuff with regard to the applied load.
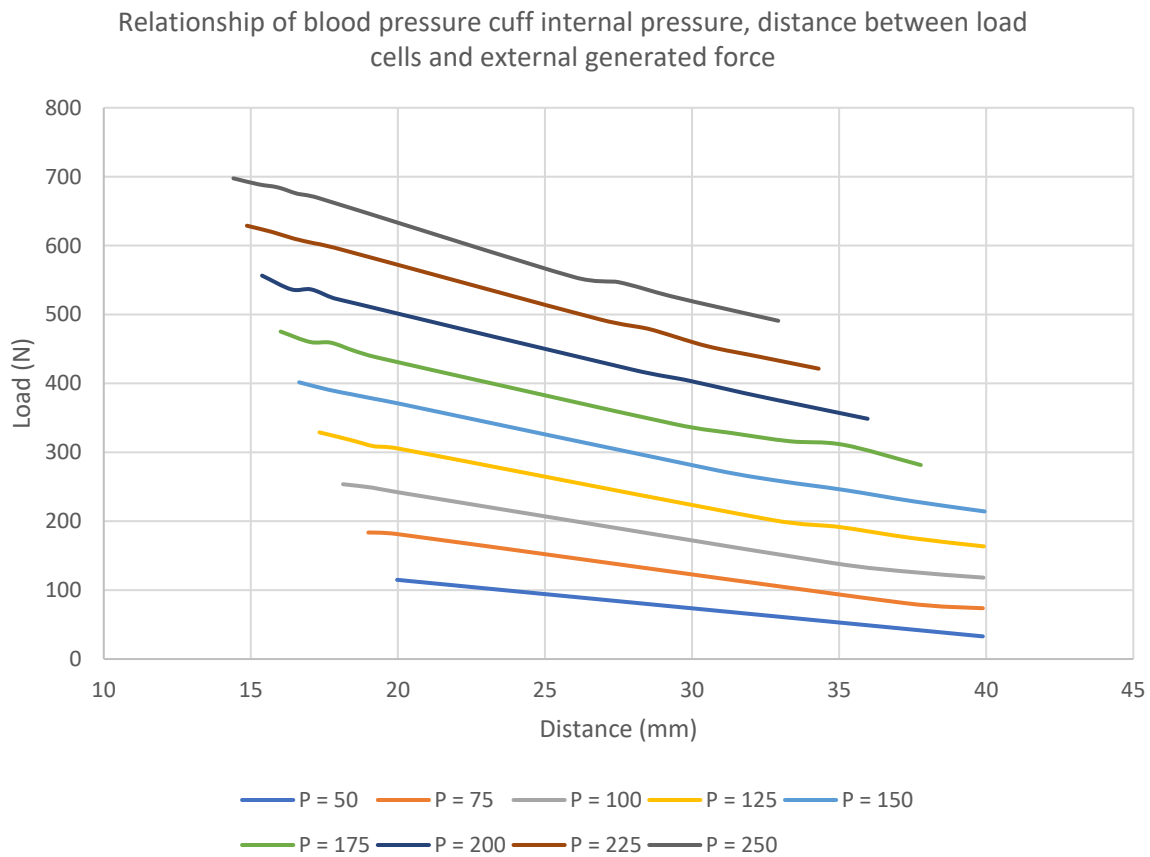
Figure 19: All lines indicate the blood pressure cuff internal pressures for a specific distance between the load cells. These are the combined results of two compression tests, the values of the compression test with an initial distance of 30 mm between the load cells is left out.

3.3 ULTRASOUND TEST

During the first brace test, one image is taken per pressure value. Figure 20 shows the ultrasound images with corresponding spinal curve automatically measured by the Scolioscan software. The purple numbers indicate the largest spinal angles measurable in the image. Around T8 in all ultrasound images an inaccuracy can be seen due to untying of the upper back strap and tying of the mid back strap of the brace, but the line describing the spinal curve still looks smooth so it does not influence the results.

The result of the 0 mmHg measurement shows a small S-shaped curve, noticeable by the two curve values given in purple. The lumbar curve is measured to 0.8° and the thoracic curve is measured to 6.3°. Increasing the pressure by 100 mmHg creates a C-shaped curve to the left side with a value of 10.4°. Increasing the pressure further by 50 mmHg creates a C-shaped curve with the apex on the right side of 13.2°. A maximum pressure of 200 mmHg creates an angle of 23.2° towards the left side. Figure 20A shows the location of the pressure cuffs creating the three point bending system.
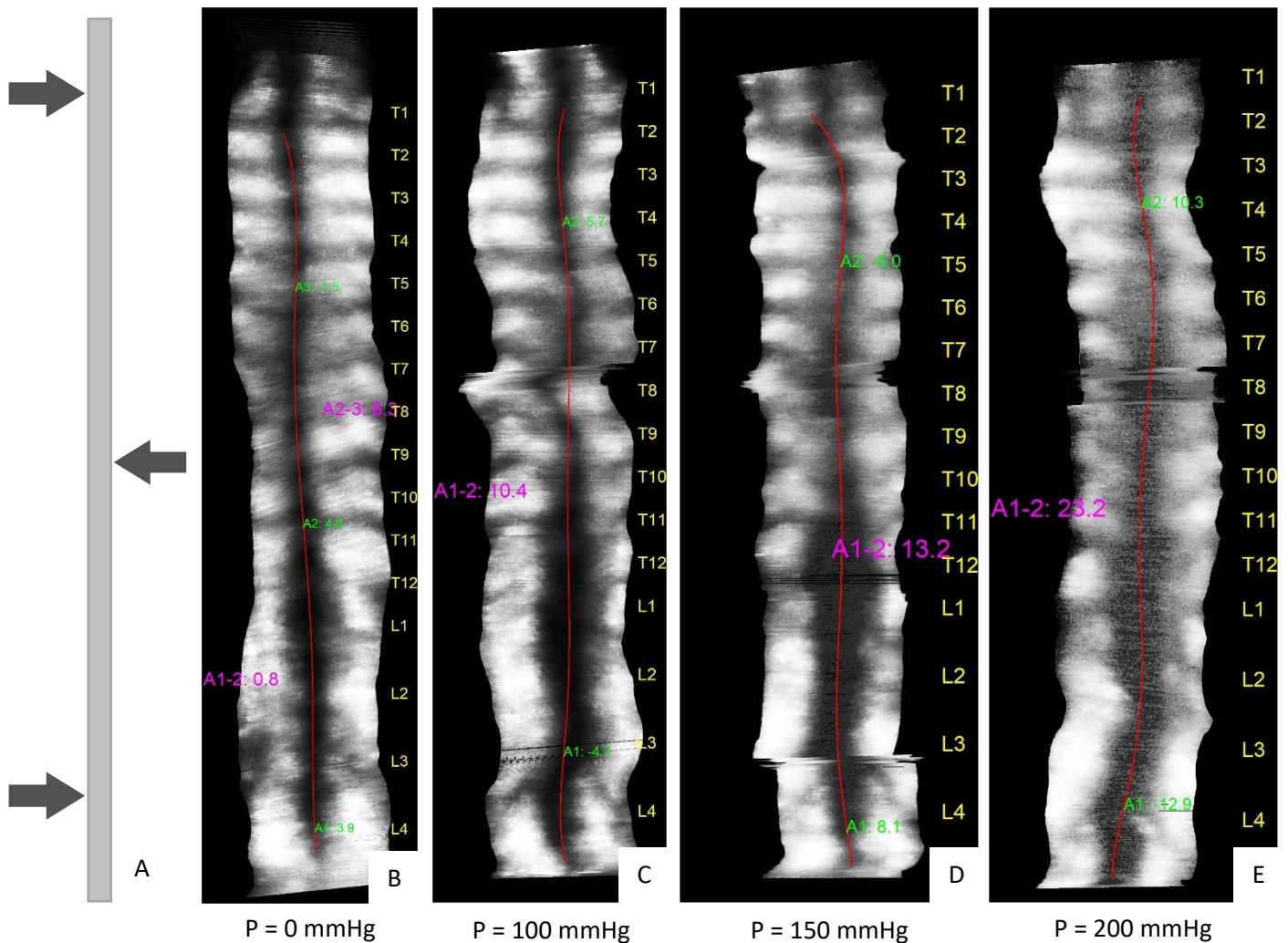
Figure 20: A: posterior visualization of the pressure area directions, creating a three-point pressure system. B-E: Ultrasound images taken right after increasing the pressure value in every meter equally. The purple values indicate the automatically measured spinal angle by the Scolioscan software. In yellow the individual vertebrae are indicated. Image B shows the result brace wear without inflation of the cuffs. Image C shows the results when all cuffs are inflated to 100 mmHg, which is increased with 50 mmHg for the following measurements.

Figure 21 shows the effect of time while keeping the pressure constant at 100 mmHg. Two ultrasound images are taken right after inflation of the cuffs, after 60 minutes and after 120 minutes. All images show a thoracolumbar curve bending towards the left side, as expected because the pressure is applied in the same way as in figure 20. Figure 21A shows a C-shaped curve, whereas image B shows an S-shaped curve while these images are taken right after each other. The values of the A1-2 curve variate between 10.6° and 21.4°. An overview of all curve angles corresponding to figure 21 is shown in table 1. No trend is discovered concerning time development and spinal curve angle. The values between repetitive measurements vary considerable as can be seen in table 1, but the location of the curves are similar in different measurements.
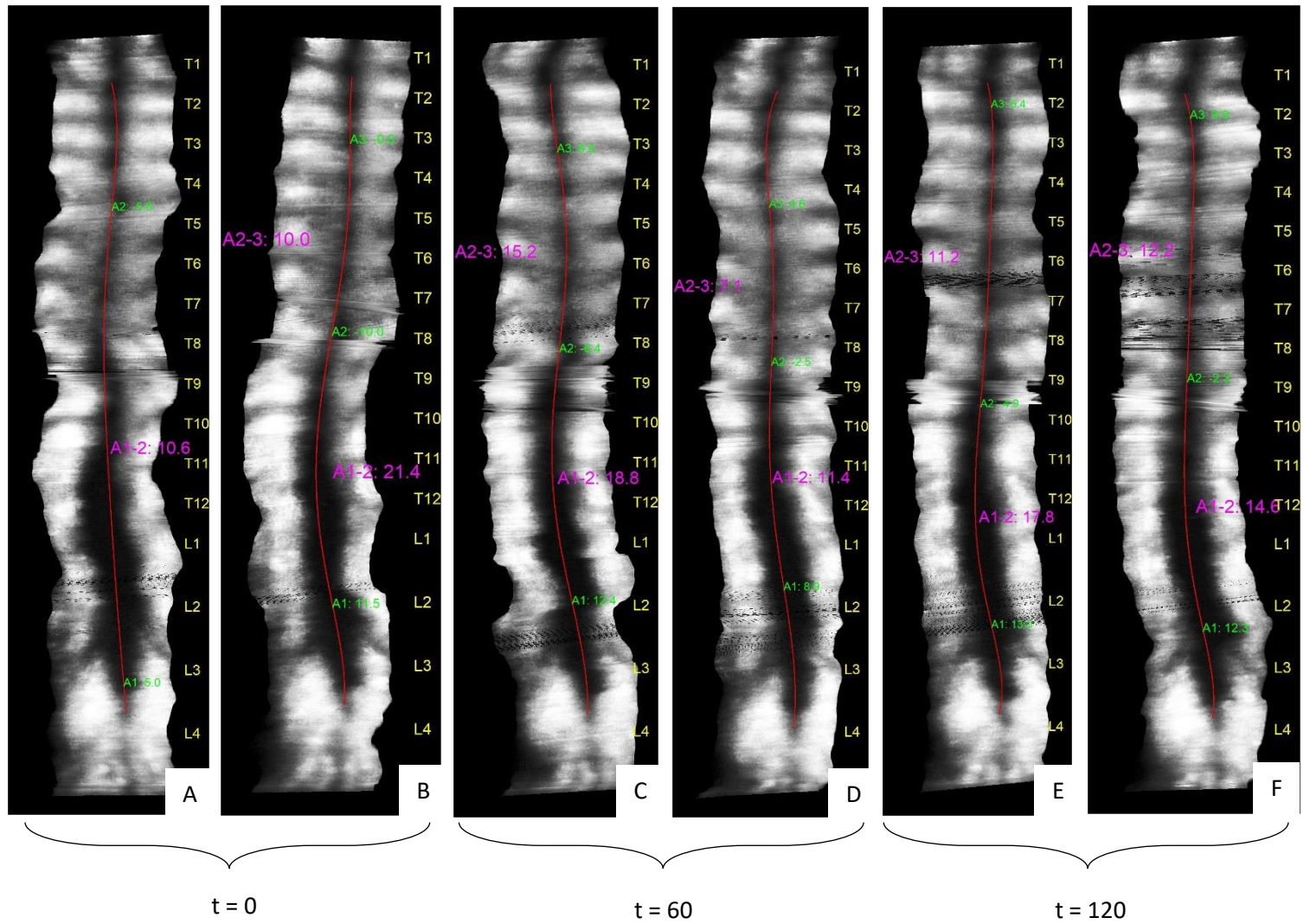
Figure 21: Posterior view of the ultrasound image results, all cuffs inflated to 100 mmHg. Image A-B, C-D and E-F were taken right after each other with a time difference of 60 minutes between them. Pressures are applied in the same direction as figure 15. A1-2 represents the thoracolumbar curve, A2-3 represents the thoracic curve.

Table 1: Measurements of spinal angle sizes, location and apex direction from figure 21.

Image	Time (min)	Pressure (mmHg)	A1-A2	Left/Right	Location	A2-A3	Left/Right	Location
Figure 21A	t=0	100	10,6	L	T11	x	x	x
Figure 21B		100	21,4	L	T11	10	R	T5
Figure 21C	t=60	100	18,8	L	T11	15,2	R	T6
Figure 21D		100	11,4	L	T11	7,1	R	T6
Figure 21E	t=120	100	17,8	L	T12	11,2	R	T6
Figure 21F		100	14,6	L	T12	12,2	R	T6

As final ultrasound test, the pressure is increased up to 200 mmHg. The aim of this test was to create an ultrasound image without inflating the cuffs, right after inflating the cuffs to 200 mmHg, after 60 minutes of inflation and after 120 minutes without altering the pressure. However, after 60 minutes

of wearing the brace, the test subject almost fainted due to the applied pressures. Therefore, the test was ceased after 60 minutes, and no ultrasound images were taken after wearing the brace for 60 and 120 minutes. Ultrasound images made at t=0 are shown in figure 22.

After 30 minutes of wearing the brace, the uncomfortable feeling of the applied pressure increased. After 60 minutes the test subject was in much pain and indicated that she almost started fainting so the experiment was halted. The cuff causing most pain was the single one on the right side of the body creating a very tight feeling. The other two cuffs created less pain as the forces were distributed over a larger area. The test subject did not experience the brace being pushed away by the cuffs, which gives the impression that the brace is rigid and stiff enough. At all time, the brace did not touch the body apart from the blood pressure cuffs which confirms a true three-point pressure system.

Table 2 shows the values of the spinal angles automatically measured by the Scolioscan software. Again, a great variance is seen between repetitive measurements. When there is only a very subtle curve to be measured at P = 0 mmHg (figure 22A-B), the values vary between 2 and 16 degrees. Figure 22A-B both show a curve bending towards the right side, figure 22C-D both show a curve bending towards the left side. This shows that the inflatable air cuffs have an effect on the spinal alignment, however the values are highly variable.

During the experiment, the test subject kept track of the possible internal pressure changes of the blood pressure cuffs (Appendix VIII). Breathing influenced the pressure values of the meters, therefore noting down the meter values was consistently done after full exhalation. For example, after exhalation the pressure value was 193 mmHg, while after regular inhalation the value was 208 mmHg. Figure 8 on page 17 shows the positioning of the meters. Meter 3 is positioned as the single cuff on the right side, meter 1 is the upper cuff on the left side and meter 2 is the lower cuff on the left side. During the study with initial pressures of 100 mmHg, the pressure in meter 2 stayed most constant compared to the other meters. Meter 1 and 3 increased at first and decreased after approximately one hour. All meters have reduced pressure value after 50 minutes. During the study with internal pressures of 200 mmHg, meter 1 and 2 remained reasonably constant. Meter 3 decreased rapidly. Comparing the same meters in both studies does not show clear similarities.

The 200 mmHg in-brace pressure measurements were compared to the stress relaxation measurements of the meters (Appendix IX). The in-brace measurements of meter 1 and 2 show similar behaviour to the stress relaxation measurements. The in-brace lines are overall positioned slightly higher, due to slightly higher initial pressures, but the curve types are similar. Meter 3 shows different behaviour in-brace than during stress relaxation measurements. Pressure decreased more rapidly during brace wear, so loss of pressure is occurring which is not due to stress relaxation of the blood pressure cuff material, but suggests viscoelastic behaviour of the body.
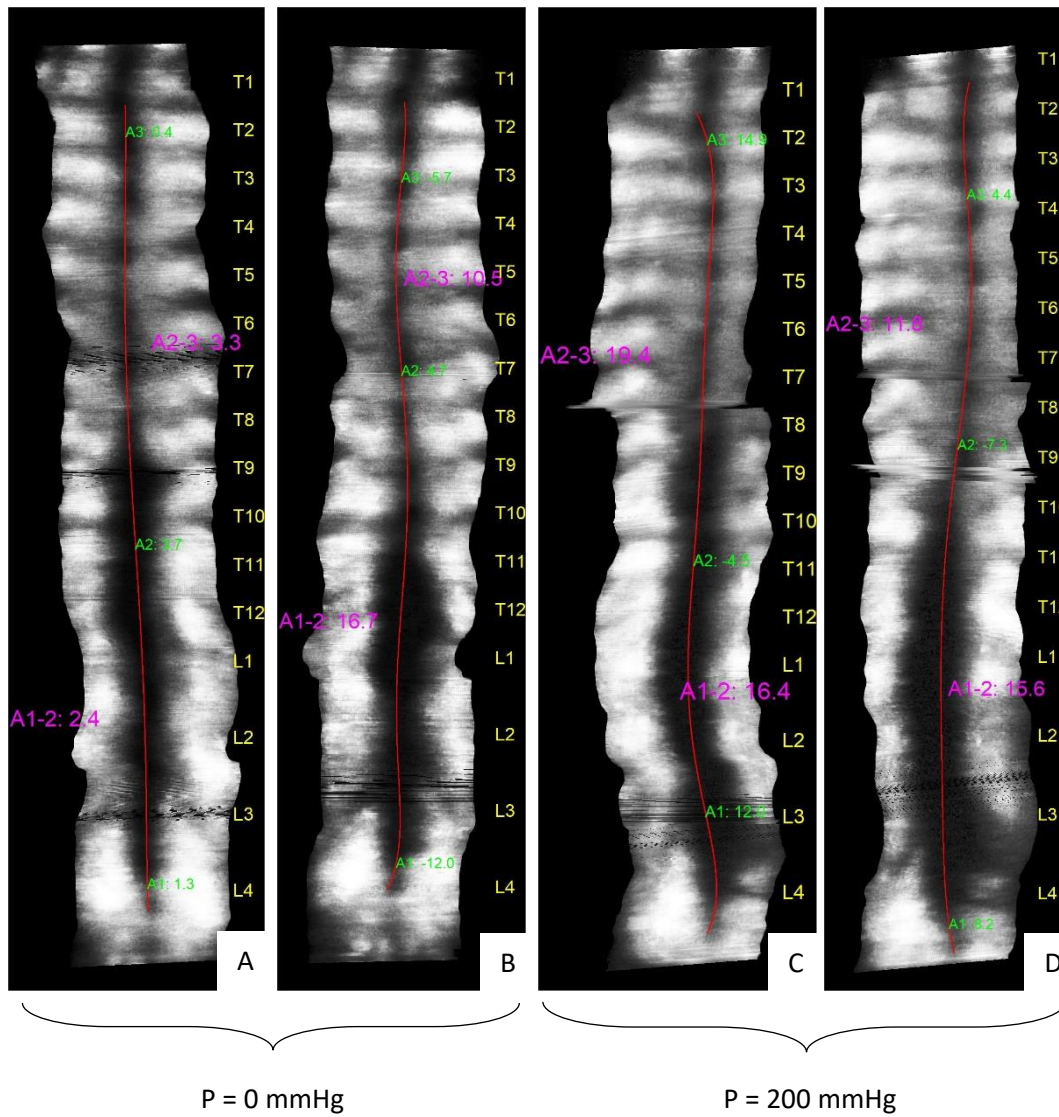
Figure 22: Posterior view of ultrasound image results, image A-B and C-D were taken right after each other. Pressures are applied in the same direction as figure 15. A1-2 represents the thoracolumbar curve, A2-3 represents the thoracic curve.

Table 2: Measurements of spinal angle sizes, location and apex direction from figure 22.

Image	Time (min)	Pressure (mmHg)	A1-A2	Left/Right	Location	A2-A3	Left/Right	Location
Figure 22A	0	0	2,4	R	L2	3,4	L	T6
Figure 22B	0	0	16,7	R	T12	10,5	L	T5
Figure 22C	0	200	16,4	L	L1	19,4	R	T6
Figure 22D	0	200	15,6	L	L1	11,8	R	T6

Figure 23 shows the free body diagram of the brace-body interaction and all individual components. The forces acting in this system are in equilibrium (equation 3.1 and 3.2). Every blood pressure cuff itself is also in equilibrium, the forces in both directions are therefore equal (equation 3.3). The sum of the forces acting on the body needs to be zero, therefore equation 3.4 holds. Equation 3.5 describes that the sum of the forces acting on one side of the body are equal to the forces acting on the other side of the body. The sum of moments acting around point A in figure 23 is also in equilibrium (equation 4.1). When P3 is exactly positioned between P1 and P2, equation 4.4 holds. Filling in equation 3.5 and 3.4 in equation 4.3, results in equation 4.5. Solving this results in $F_{A2} = F_{B2}$.

Figure 23 describes two situations, in situation A there is equal distance between the body and brace on both sides, $l_1 = l_3$. In situation B the distances are not equal, $l_1 < l_3$. In both situations there is a force equilibrium. In situation A it is not possible for all internal pressures to be equal, so $P_1 = P_2 \neq P_3$. The force acting on the body is related to the distance between the body and brace. Knowing the distance between body and brace and the internal pressure in the cuff gives one specific load value (figure 19). Keeping all pressures equal when $l_1 = l_3$ does not result in a force equilibrium in situation A. Figure 23B describes the situation during testing of the brace. In this situation it is possible for all pressures to be equal, $P_1 = P_2 = P_3$. Length l_1 is smaller than l_3, which causes higher forces acting on the body for equal internal pressures. This is due to an increase in surface area of the P_3 blood pressure cuff making contact with the body and brace. The contact area of the P_1 and P_2 blood pressure cuffs decrease.

An example of possible pressure values for situation 23A and 23B is given in table 3, obtained by figure 19. This shows that the load applied at the experiment when using 100 mmHg for all meters, is maximally 250 Newton, assuming that the distance between the brace and body is at least 20 mm. The load is at least 170 Newton, which is the pressure value linked to a distance of 30 mm. As the distance between brace and body summed for both sides is 60 mm, the minimum of 30 mm is achieved on at least one side. This load of 170 Newton is higher than achieved pressures in literature. Because of the variety in ultrasound measurements, it is needed to use a more accurate measurement technique. Therefore, additional boneMRI's are needed.

$$\sum F_x = 0, \sum F_y = 0 \qquad \text{Eq. 3.1}$$

$$F_{A1} - F_{A2} + F_{B1} - F_{B2} + F_{C1} - F_{2C} = 0 \qquad \text{Eq. 3.2}$$

$$-F_{A1} = F_{A2}, \ F_{B1} = F_{B2}, \ F_{C1} = F_{C2} \qquad \text{Eq. 3.3}$$

$$F_{C1} - F_{A2} - F_{B2} = 0 \qquad \text{Eq. 3.4}$$

$$F_{C1} = F_{A2} + F_{B2} \qquad \text{Eq. 3.5}$$

$$\sum M_A = 0 \qquad \text{Eq. 4.1}$$

$$F_{C1} \cdot h_2 - F_{A2} \cdot h_1 - F_{B2} \cdot h_3 = 0 \qquad \text{Eq. 4.2}$$

$$F_{C1} \cdot h_2 = F_{A2} \cdot h_1 + F_{B2} \cdot h_3 \qquad \text{Eq. 4.3}$$

$$h_1 = 2(h_2 - h_3) + h_3 \qquad \text{Eq. 4.4}$$

$$(F_{A2} + F_{B2})h_2 = F_{A2}(2(h_2 - h_3) + h_3) + F_{B2} \cdot h_3 \qquad \text{Eq. 4.5}$$

$$F_{A2}(h_3 - h_2) + F_{B2}(h_3 - h_2) = 0 \qquad \text{Eq. 4.6}$$

$$F_{A2}(h_3 - h_2) = F_{B2}(h_3 - h_2) \qquad \text{Eq. 4.7}$$

$$F_{A2} = F_{B2} \qquad \text{Eq. 4.8}$$

Table 3: Possible parametric values of situation A and B from figure 19. In situation A, $l_1 = l_3$ which is always 30 mm because L and l_2 have fixed values. In situation B, $l_1 + l_3 = 60$ mm, because of the fixed values of L and l_2.

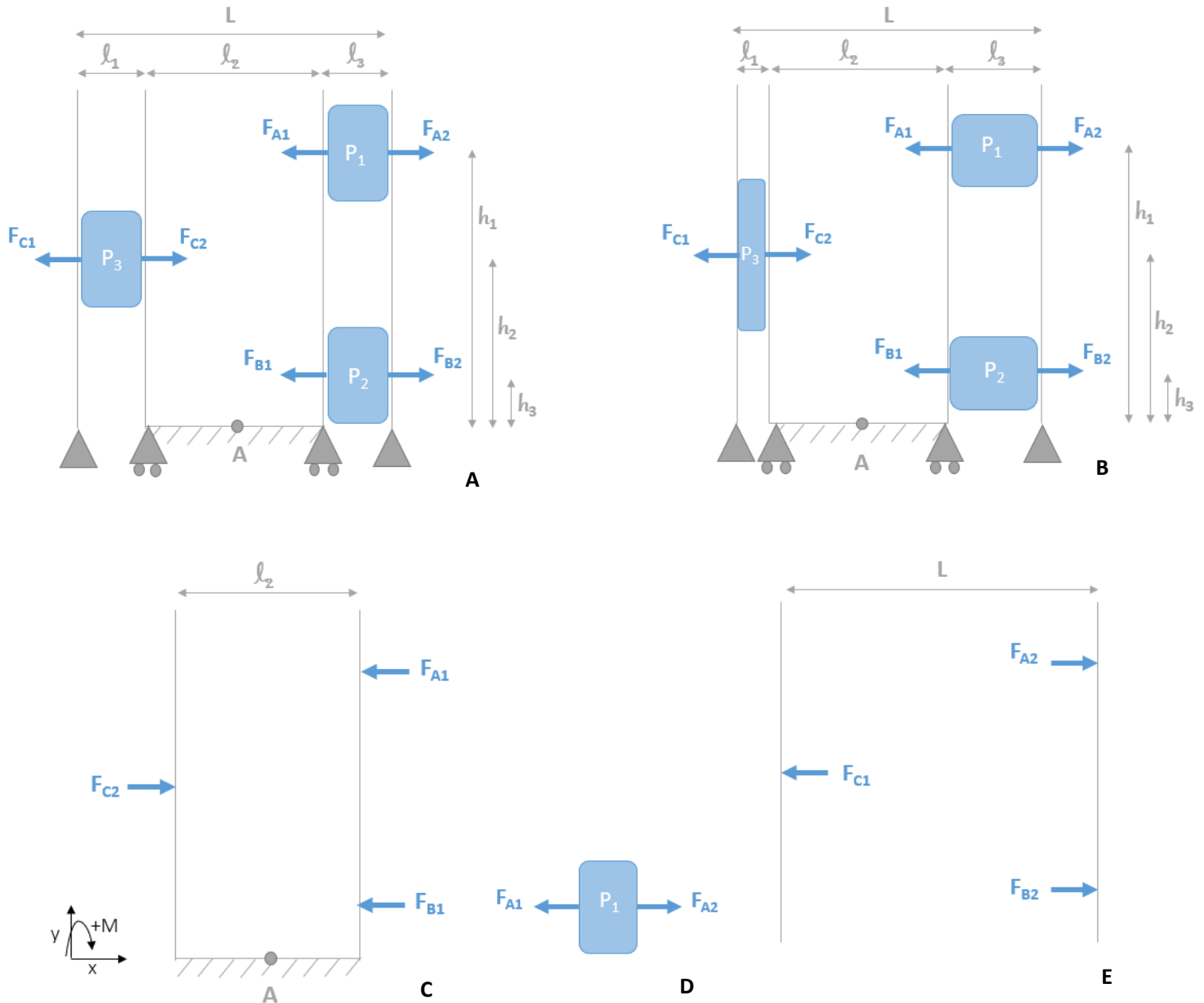|	Situation A	Situation B
P_1 and P_2	100 mmHg	100 mmHg
P_3	175 mmHg	100 mmHg
F_A and F_B	170 N	125 N
F_C	340 N	250 N
l_3	30 mm	40 mm
l_1	30 mm	20 mm

Figure 23: Free body diagram (FBD) representation of the brace-body interaction. The blood pressure cuffs are visualized in blue, l_2 represents the body width and L represents the brace width. The gravitational forces are neglected in this situation. Image A and B indicate situations with different distances between the brace and body which is possible in real life and influences the pressure inside the cuffs. Image C, D and E represent the FBD of the body, cuff and brace respectively. Length L and l_2 are fixed. F_{A1}, F_{B1} and F_{C2} indicate the forces acting on the body, caused by the blood pressure cuffs. This situation is in equilibrium and the sum of the forces acting in x-direction is zero. Every blood pressure cuff is also in equilibrium which means $-F_{A1} = F_{A2}$, $-F_{B1} = F_{B2}$, $-F_{C1} = F_{C2}$. In situation A, $l_1=l_3$, in situation B, $l_1<l_3$. P_1-P_3 indicate the pressures in the blood pressure cuffs.

3.4 MRI TEST

The internal pressures of the blood pressure cuffs were documented to keep track of possible changes (Appendix X). All meter pressures fluctuate around 100 mmHg but stay relatively stable, and no significant change is visible after one hour which is different from the ultrasound tests.

Projection images of the three boneMRI measurements are visualized in figure 24. At first glance a subtle difference in spine alignment can be seen between figure 24A and B, while figure B and C look very similar. Figure B shows a small S-curve with the apex of the curves being around T6 and T12. This would mean that the transitional zone is located around T9. The mid-cuff is located at the right side of the body and puts pressure on the lower ribs which translates diagonally upwards through the body.

To get a clearer image of the three-dimensional deformity, segmentations of the spine are visualised in figure 25. In anterior and posterior view, a small deformation is visible after applying pressure.

P = 0 mmHg, t = 0   P = 100 mmHg, t = 0   P = 100 mmHg, t = 60 min
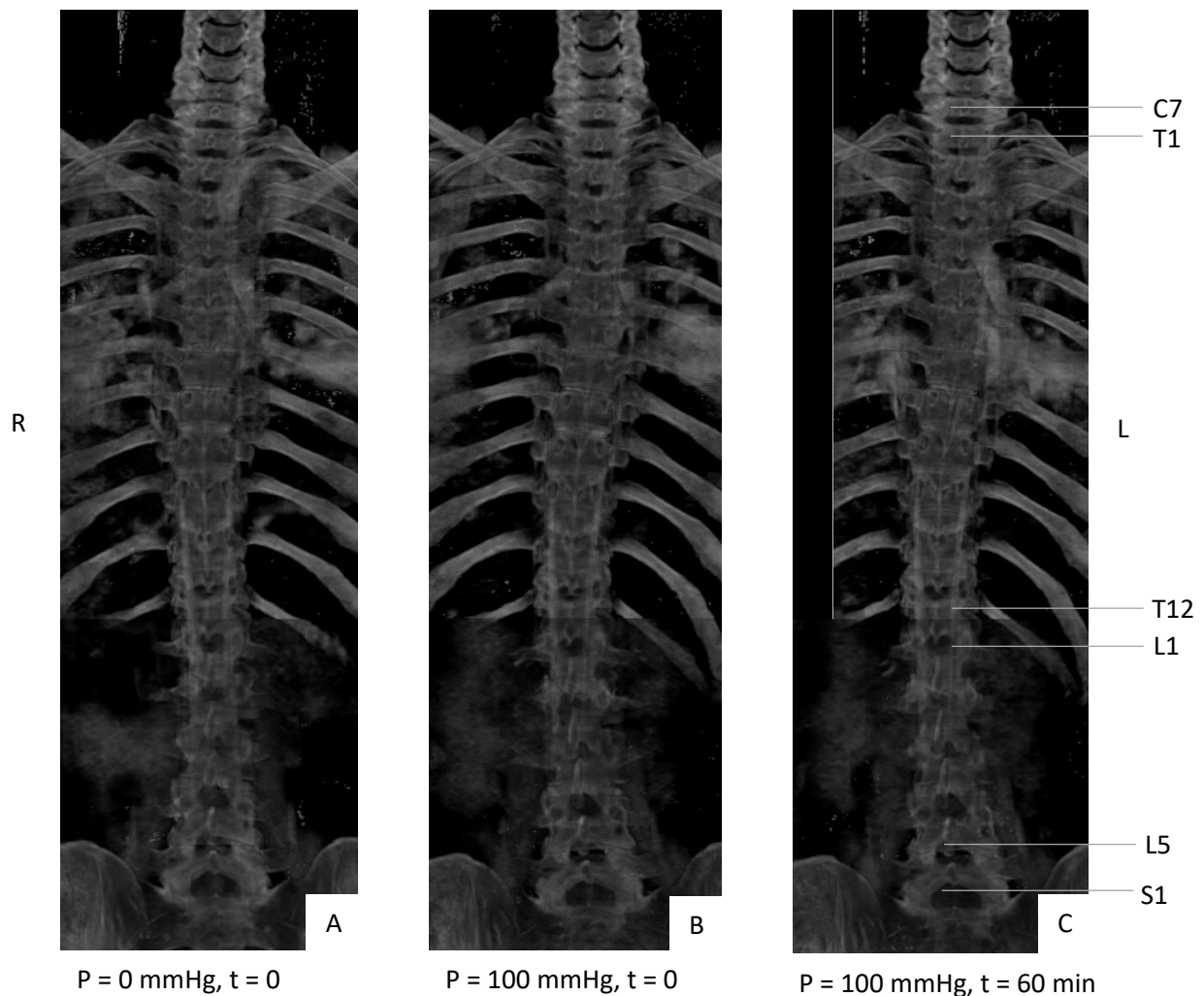
Figure 24: Projections of the boneMRI's. Image A shows the neutral measurement without inflation of the cuffs. Image B has three inflated cuffs, taken right after inflation. Image C is taken after one hour of inflation. R and L represent the left and right side of the body, the sacral, lumbar, thoracic and cervical vertebrae are indicated. The mid-cuff is positioned at the right side of the body.
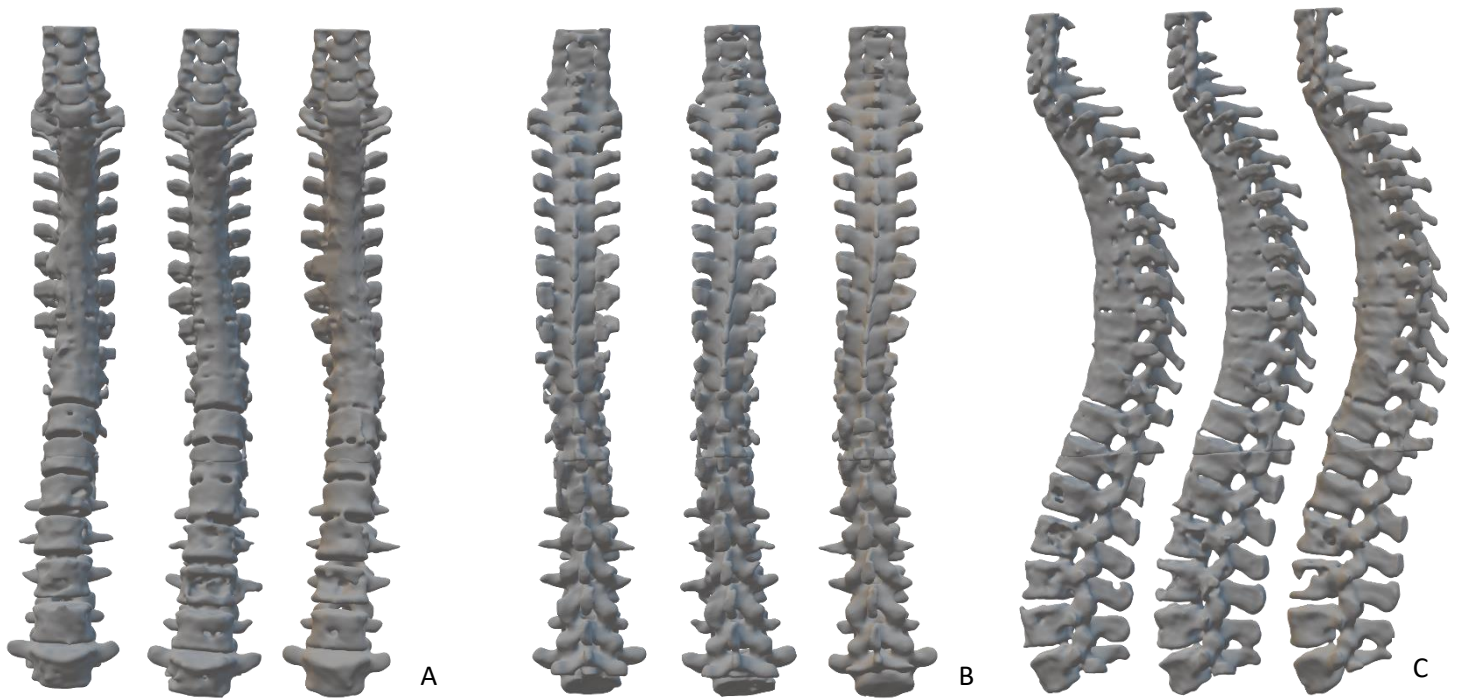
Figure 25: Segmentations of the boneMRI's. Image A shows the anterior view, B shows the posterior view and C the lateral view. For every view the order of images (from left to right) is: without pressure, with pressure, with pressure after one hour.

Table 4 shows the left-right measurement taken of the total spine, of all discs and of all vertebrae. Noticeable is the difference in total length between the measurements with and without inflated cuffs. Without pressure on the spine, the total length is smaller. Both the vertebrae and the discs are of influence in the increase in total length.

For all situations, the disc length is higher at the right side and the vertebral length is higher at the left side. There is a minor difference between the measurements right after applying pressure and after one hour of pressure, looking at the length of the right side of the disc and vertebra. Immediately after applying pressure, the distance between the discs is smaller on the right side than after waiting for one hour. The vertebrae decrease equally in length after applying pressure for one hour. Most pressure is applied at the right side of the body as this is where the mid-cuff is located. Furthermore, there is no significant difference between left-right measurements for the discs and vertebrae between the different studies.

Table 4: Left-right length measurements for the total spine, per intervertebral disc and per vertebra, for three MRI's in mm.

	Total length left	Total length right	Disc length left	Disc length right	Vertebral length left	Vertebral length right
P=0	381	382	105	108	277	275
P=100 t=0	388	386	108	110	279	276
P=100 t=60	388	386	109	113	279	273

Table 5 shows the anterior-posterior length results of the total spine, the intervertebral discs and the vertebrae. Again, the total length of the spine is larger after applying pressure, both anterior and posterior. There is no significant difference between measurements for as well the anterior as the posterior length. The posterior length of the disc increases after applying pressure for one hour, while the posterior length of the vertebra decreases after one hour.

Table 5: Anterior-posterior length measurements for the total spine, per intervertebral disc and per vertebra, for three MRI's in mm.

	Total length anterior	Total length posterior	Disc length anterior	Disc length posterior	Vertebral length anterior	Vertebral length posterior
P=0	389	369	118	92	271	277
P=100 t=0	392	372	121	92	271	280
P=100 t=60	392	374	121	98	271	276

Table 6 shows the mechanical torsion measurements. The total torsion is similar for the first and third measurement, but right after increasing the pressure the rotation is higher. This suggests recovery of the spine towards an equilibrium. For all measurements the vertebral rotation is approximately 10 percent higher than the disc rotation.

Table 6: Mechanical torsion measurements summed for the total spine, all intervertebral discs and vertebrae in degrees.

	Total rotation	Total disc rotation	Total vertebral rotation
P=0	182	87	96
P=100 t=0	226	107	119
P=100 t=60	172	81	92

To discover a possible trend in mechanical torsion over the complete spine, the rotation values are compared for every individual disc and vertebra. All graphs can be seen in Appendix XI. There is not one region in the spine where the rotation is higher or builds up, compared to other regions.

Similar shaped graphs can be seen after applying pressure, as the peak values are located at comparable spine areas. Without inflation of the cuffs, the rotation inside the vertebrae and discs fluctuates less, as this line is slightly smoother.

As the apex of the curves are estimated around T6 and T12, the left-right lengths are featured for these apical regions in Appendix XII. There is no clear difference in left-right length for the discs and vertebrae at both apical regions. The transitional segment (T9) between the apical regions does not show more mechanical rotation (Appendix XI). In fact, it shows a lower rotation than surrounding vertebrae.

4

DISCUSSION

4.1 GENERAL FINDINGS

The results will first be discussed in general followed by a more detailed discussion per experiment in every subsection.

As a preparation on the ultrasound and MRI experiments three blood pressure cuffs were selected that did not show any stress relaxation. The goal of conducting the compression tests was to find a relationship between internal pressure of the blood pressure cuff and the external load it creates. This relationship relates to the distance between the load cells which can be compared to the situation in real life where the distance between the load cells mimics the distance between the brace and the body. It is very hard to determine this distance when wearing the brace and therefore the exact loads acting on the body. It is possible to give a rough estimation of generated loads, as the distance between the body and brace is always at least 30 mm on one side, at least 170 Newton of load is created when using 100 mmHg pressure in all cuffs.

During ultrasound measurements, a loss of pressure was measured for both the 100 mmHg and the 200 mmHg test. This could indicate creep behaviour of the body, as stress relaxation of the cuffs is excluded.

The ultrasounds images show varying results so it can only be concluded that the pressure cuffs do cause a change in spinal alignment but the magnitude remains questionable. Spinous processes (SPs) and transverse processes (TPs) can be used to measure a coronal deformation through ultrasound imaging. These techniques can give an indication of curve severity, but use different landmarks. In the study of Brink (2017), the thoracic and (thoraco)lumbar coronal ultrasound angles were 23%-37% and 15-27% lower as compared with radiographic Cobb angles [35]. A difference is expected, as the landmark used for Cobb angle is the vertebral body, which is more anteriorly located than the landmarks used for ultrasound measurements. This leads to a different projection of the 3-dimensional deformity. The Cobb angle is a simplification of the complex 3-dimensional deformity, and therefore not necessarily more useful than spinal angles obtained through ultrasound measurements. Excellent linear correlations were discovered between all ultrasound angles and the Cobb angle. The inter- and intra-observer errors of ultrasound angles were recorded by the mean absolute difference, which had a maximum of 5° [35]. This means that a deviation of 5° of the true spinal angle is possible for ultrasound measurements.

The in-brace ultrasound test is executed on a non-scoliotic patient, in the hope of creating a minor scoliotic curve. The possible ultrasound deviation of 5° has a larger influence on smaller spinal curves. A spinal curve of only 5° could be calculated as a 0° or 10° curve. For this research ultrasound imaging might not be the most accurate way of determining coronal curves.

Moreover, measuring the SP angle automatically gives better results for larger spinal curves. This is due to the Scolioscan software seeking a curve, which might not be existing. This is evident when looking at figure 20. At the highest section of the red line, a strong bend can be seen. This line is an exaggeration of the true spinal angle. However, this strong bend is taken into account when measuring the automatic SP angle, which causes a greater spinal curve to be measured. This is not the case for larger spinal angles, which makes this method more suitable for larger scoliotic curves.

Measuring the SP or TP angle by hand would be an option as an alternative for the automatic measures, but the quality of these ultrasound images is too low to determine the spinal angle accurately. Especially the lumbar part shows a vague dark area. This can be due to the test subject being older than the average patient using the Scolioscan, and therefore containing more soft tissue at lumbar areas which creates more distance between the spine and ultrasound head. It can also be caused by contraction of the back muscles as a reaction of wearing the uncomfortable brace.

Moreover, the aim was to create a scoliotic curve for a healthy subject. This is challenging as the subject is less flexible than the average adolescent scoliotic patient because of the age difference. Furthermore, it is assumed that restoring spinal balance in a scoliotic spine is easier than creating a spinal curve in a straight back. Vertebral wedging is present for scoliotic patients, which creates more triangular shaped vertebrae [53]. Block like vertebrae of a healthy subject are aligned well and it is therefore harder to enforce a curve. Moreover, this research has only been executed on one subject as it serves just as a proof of concept, but it makes the results less reliable than for a large cohort study.

In literature some measurements were taken to estimate the forces acting on the body. A study by Chung (2018) tested a dynamic brace with pad pressure forces acting on the body of maximally 46 N [54]. Perie (2005) revealed that forces acting on the body of 58±18 N were common when wearing a Boston brace [51]. Forces up to 100 N were measured in the Milwaukee and Boston brace. The forces used in our study were at least 170 Newton which is higher than used in literature. For future studies on scoliotic patients it is preferred to use a lower force, more similar to values used in literature for safety.

Spinal curves measured while standing are more accurate than measured under other postures [46]. Lying down eliminates the axial forces on the spine because of gravity. The spinal angles can therefore be smaller when measuring in supine position [55]. This underestimation also counts for axial rotation of the vertebrae [56]. This makes MRI less suitable for measuring spinal curves and determination of the correct pressure pad location for a day time brace. MRI is more beneficial for determination of the pressure pad locations of night time braces, because of similar positioning of the body. This could explain why the size of the spinal curve looks larger when analysing the upright performed ultrasound measurements.

In a study of Brink (2017) the thoracic curve was underestimated by 12°-14° in supine position compared to upright position for high scoliotic curves in coronal plane [56]. Increased Cobb angles also increased the underestimation in supine position. For small spinal curves dealt with in our study, this difference is therefore smaller.

The study of Schlösser (2014) found that scoliotic patients have at least three times more torsion, anterior overgrowth and coronal wedging in their discs than in their vertebrae. They described AIS mainly as a deformity of the intervertebral discs, with adaptive behaviour of the bony structure. Anterior overgrowth and coronal asymmetry were greatest at apical regions, whereas torsion was most apparent at transitional segments between curves [52]. The apical region was defined as the

apical vertebra plus the adjacent segments above and below. This study was executed on high resolution CT scans, with a measurement error of 0.1°/cm for torsion, and 0.2 mm for measuring distances with the ScoliosisAnalysis software [52]. Using lower quality boneMRI data, a higher error is expected. In our study, the apical regions do not show coronal asymmetry and there is not more torsion apparent at transitional segments. Because of the small spinal deformity, it is challenging to define the apex of the curves.

The mid blood pressure cuff is located at the right side of the body, putting forces on the lower ribs. This horizontal applied force gets translated diagonally upwards because of the orientation of the ribs, which creates an S-curve thoracically. The curve therefore lays more thoracic than where pressure is applied. This could be the cause of the spine to lengthen when applying pressure, as the force effect is not purely horizontal. Increasing the spinal length could be beneficial when trying to correct spinal curves, as this creates more room between vertebrae and therefore enables room for changes in the spinal alignment. The fact that the total length of the spine is approximately equal for the left and right side is expected, as an S-curve is created. When only a C-curve is apparent, coronal wedging is caused at one side.

The only significant difference between the measurement with pressure applied immediately and after one hour is the axial rotation. The axial rotation increases after increasing the pressure, but decreased after one hour. The increase in axial rotation is explained by the increase in pressure, the decrease in rotation could be explained by the spine reaching an equilibrium due to viscoelastic behaviour. Rotation was expected to be higher in the intervertebral discs, as scoliosis is mainly a deformity of the discs [52]. This is not the case in our study, as the vertebral rotation is higher.

4.2 STRESS RELAXATION MEASUREMENTS

It is expected that the values of the meters stay equal or decrease slightly due to the elasticity of the blood pressure cuffs. The amount of air in the cuff is expected to stay equal, but the material can deform which changes the volume and can cause a change in pressure. To prevent or minimize this behaviour, there is a textile case around the cuffs. However, the rubber like material of the cuff might still be able to reshape within the textile case and the tubes might still show viscoelastic behaviour.

Temperature could be of influence on possible viscoelasticity of the rubber, and on the pressure inside the cuffs. According to Gay-Lussac's law the pressure is directly proportional to absolute temperature at a constant volume and fixed mass of gas [58]. Equation 5 shows that a difference of 5 degrees Celsius has small impact in pressure change.

$$\frac{P1}{T1} = \frac{P2}{T2}$$

Eq. 5.1

$$\frac{200\ mmHg}{293\ K} = \frac{P2}{298\ K}$$

Eq. 5.2

$$P2 = 203\ mmHg$$

Eq. 5.3

The volume might change due to the viscoelastic behaviour of the rubber and due to possible pressure changes. All tests were executed in the same environment assuming under equal conditions. However, no temperature measurements have been taken. Moreover, if the temperature had influence on one test, this should be visible for every meter. Looking at the graphs, there is not one test which shows atypical behaviour for every meter. This scenario is therefore excluded.

The reason for the variable outcomes per meter can be due to a flaw in the gauge or pump. After execution of a test, the pressure is released by opening the pressure release valve. At least one hour of waiting is calculated between measurements. The pressure release valve is closed again to start the new experiment. This variable is changed in between measurements and could therefore be of influence on the results. Moreover, at least one hour of waiting was chosen between measurements to avoid experimenting on pre-stretched material. This time-interval was different between all measurements and could therefore also be of influence.

Another flaw in this experiment is reading the pressure values of the gauges. All six gauges were aligned next to each other in order for the camera to image them all. The two gauge meters centrally located were filmed exactly from front view. However, the outer gauge meters were filmed under an angle which caused a distorted image. The values of the gauges placed on the left side were underestimated and the gauges placed on the right side were overestimated. The positioning of the meters and camera angle did not change between measurements, this is therefore not taken into consideration when values of a meter showed atypical behaviour. Comparisons between data points of one meter show the same under- or overestimation if present.

4.3 COMPRESSION TESTS

The lines in figure 19 show the results of the two compression tests combined. Appendix VI shows the results of all tests. The cause of the small drop in load between 25-30 mm is unclear. It could be explained by a difference in surface area touching the load cell. The dimensions of the cuff change differently when a distance is smoothly changed than when it is changed rather abrupt for example as initial distance. Figure 19 is therefore an approximation of the loads acting on the body. When the internal pressure is equal but the external created load is higher due to a smaller distance between load cells, the surface area is increased.

The compression test with an initial displacement of 40 mm can achieve a Δ displacement of 10 mm, which causes a net displacement of 30 mm. No interpolation was therefore needed in Appendix VI between these compression tests. The compression test with an initial displacement of 30 mm never reaches a distance of 20 mm. Interpolation between these tests is done in order to create a continuous smooth line but again creates an approximation of loads acting on the body, same holds for figure 19.

During execution of a compression test, the pressure inside the blood pressure cuff was filmed to keep track of changes. After collecting the data (load, time and displacement), this was linked to the internal pressure values. The videos showed the internal pressure values on a specific time of filming. By coupling the time of the videos with the time of the experiment, the internal pressure can be related to the displacement and load. However, the duration of the compression test was not always exactly equal to the video. It is possible that not all pressure values were matched correctly to the time in the video. Assuming the difference will be maximally 5 seconds, this does not influence the results considerably.

It was challenging to read the pressure values from the gauges precisely, as the quality of the videos did not allow to see the individual values on the meter. However, the deviation is estimated on a maximum of 2 mmHg which is not consequential for this research.

4.4 ULTRASOUND TESTS

The first executed ultrasound test (figure 20) shows unexpected results for the P = 150 mmHg measurement. The apex of the curve is measured towards the right side, which is the side where most pressure is applied. This can be caused by irregularities in the ultrasound image. Around L3 there is an inaccuracy due to shifting of the ultrasound head. The increase in pressure did also increase the spinal curve which is expected. This ultrasound test is executed by a different researcher than the other tests. This can be of influence for the results as the quality of ultrasound imaging is highly dependent on the skill and experience of the person taking the images [59].

For the second test, measurements were repeated to validate the reliability of this measurement technique for small curves. All thoracolumbar curves in figure 21 are located at the same height and pointing towards the same direction which is expected as the positioning of the blood pressure cuffs was not changed. Five out of six images create an S-shaped curve which is due to changes in the lower part of the spinal alignment influencing the upper part as well. The values of the automatic measurement show highly variable results between repetitive measurements which can be due to the 5° inaccuracy. It is therefore not possible to draw conclusions from the spinal curve angles and especially the influence time has on the curve. It can only be concluded that the brace caused a spinal angle, compared to not wearing a brace, because of the apex of the curve pointing towards the left in every image when applying pressure versus pointing to the right without applying pressure.

The final ultrasound test (figure 22) shows that a curve is created towards the left side after applying a pressure of 200 mmHg. The curves created are not higher than the 100 mmHg pressure test, an increase in curve is expected as the forces acting on the spine are larger. The neutral measurements show highly variable results between 2.4° and 16.7°, but both lumbar curves pointing towards the right. The net angular difference is therefore higher than just the spinal angle achieved after applying pressure because a curve in opposite direction is created. Again, it can only be concluded that the pressure cuffs do cause a change in spinal alignment but the magnitude remains questionable through ultrasound measurements.

For one experiment, the blood pressure cuff location was not changed. However, between experiments the blood pressure cuffs were taken off and repositioned to the original location. It is possible that the cuffs are not exactly positioned equally. Moreover, the cuffs are not rigid and take their shape through the body. The different ultrasound measurements show an approximation of equal positioning of the blood pressure cuffs. In all experiments, the cuffs were inflated simultaneously.

Looking at Appendix VIII, it is expected that when one pressure value changes, the other values change as well. The brace, thorax and pressure pads function as one system, all influencing each other. This is visible in the graph, when certain values increase, some others decrease. The behaviour of the meters is different for both tests, which makes it challenging to draw conclusions from the data. At the end, the pressure in meter 3 decreased most in both tests which is the meter exerting most force on the subject. This causes the body to adapt, which can therefore create more space between the brace and the body which decreases pressure. Appendix IX shows a comparison between the stress relaxation

behaviour and the in-brace tests. Meter 1 and 2 show similar curves for the in-brace test and the stress relaxation test. Meter 3 shows a larger decay in pressure when wearing the brace, which means that the loss of pressure is not caused by the material properties of the cuff, but likely by adaptation of the body.

4.5 MRI TEST

The brace is not visible on the boneMRI because it is outside of the scanning region. It is therefore not possible to measure the distance between the body and brace, which gives more insight in the forces acting on the body.

The threshold for significance of changes in length, both anterior-posterior and left-right was not determined beforehand. Differences in lengths are within a few millimetres, which can be due to coronal wedging or due to measurement inaccuracies. It would be easier and more accurate to determine the lengths and rotation for larger scoliotic curves.

Semi-automatically drawing of the vertebral body and spinal canal, and determination of the landmarks was challenging when areas of the boneMRI showed lower resolution or artefacts. When there was not a complete visualization of the vertebral body and canal possible, the chosen landmarks were an estimation of the true positioning. Measurements were taken at the inferior and superior endplates of the vertebrae. In some cases, the endplates were not flat but concave, so thinner towards the centre of the vertebra in both lateral and anterior view. The endplate positioning in both views was then chosen to be as close to the maximum as possible, while still being able to see the contours of the spinal canal and vertebral body in the transverse plane. This was consequently done throughout all vertebrae measurements, but in some cases it could lead to an underestimation of the total length of a vertebrae.

A change in the length of the vertebral bodies was not expected, as this is the stiffest part of the spine and therefore likely a measurement inaccuracy. The right sided increase in disc length after applying pressure for one hour could be explained by the discs first being pushed from the right side which creates a curve directed leftwards. This causes wedging of the discs, which after one hour of wearing the brace decreases.

5
RECOMMENDATIONS

The goal of this study was to test whether it is possible to design a method to optimise the brace manufacturing without exposure to ionizing radiation. This study was executed on a non-scoliotic subject, by creating a curve in a straight spine. This study served as a proof of concept and shows that it is possible to use a test brace while doing US and MR measurements.

In this case the test brace is developed as a method to optimise the manufacturing process of a daily worn static brace. The test brace has a patient specific fit, which is time consuming to realise for multiple scoliotic patients. For the ultrasound measurements it would be beneficial to design a frame which fits every patient. The geometry and location of the pressure areas needs to be easy to adjust, same counts for the amount of applied pressure. As ultrasound is performed upright, less expensive than MRI and gives immediate results, this is preferred over MRI. For the ultrasounds study, it is possible to add pressure sensors between the pads and the body, the get a more accurate value of applied forces.

When improving the MRI study, the quantity of the pressure pads can be increased while decreasing the size of them. More and smaller pressure pads can create different pressure patterns to eventually determine the optimal pressure pad pattern. It will be challenging to find a non-personalized brace that fits every patient to execute MRI tests on, when the brace would serve as a method to determine the optimal pad pressure and location. It would be possible to create multiple standard sizes, or use the readily available Boston brace modules. The use of MRI in future research will be favourable when designing a night-time brace. Moreover, it would be favourable to use cuffs that can be inflated from a distance, without the need for tubes. However, making this MRI compatible is challenging.

In this study the decrease of forces acting on the body has not been proven. This needs to be tested on a larger time period for scoliotic patients, like the study of Lou (2012). If the forces decrease due to changing spinal alignment, patients could benefit from a dynamic firm fitted brace. This can keep the forces constant by changing the size of the pressure pad. A feedback system would be needed to measure the forces acting on the body and ideally a pressure pump would regulate the amount of air inside the cuffs, to retain constant forces. This could prevent the correction from decreasing and make the brace more effective by retaining the effect of the initial correctional. Moreover, small inflatable pressure pads can be applied over the whole brace-body surface to make every pressure pattern possible. Another simpler option would be to automatically adjust the strap tension on the backside of the brace to keep the forces acting on the body constant, since strap tension and pad pressure strongly correlate [47]. However, adjusting the strap tension only changes the magnitude of the forces, not the direction and size of it.

It would be beneficial to execute the same experiments on a scoliotic patient, now that the method has proven to be save. Only after execution on scoliotic patients, the method can be proved effective.

6

CONCLUSION

The manufacturing of scoliotic braces is an ineffective process, which results in a suboptimal end product. This study serves as a proof of concept with the goal to improve the effectiveness of brace treatment for adolescent idiopathic scoliosis patients.

The blood pressure cuffs were mechanically tested on viscoelastic behaviour and compression tests were executed to determine a relationship between internal pressure and external created loads. No stress relaxation was discovered in the cuffs and the forces acting on the body are estimated to be between 117 and 242 Newton per cuff, which is more than used in literature.

The experiments were performed on a non-scoliotic subject, with the aim to create a spinal curvature. Both US and boneMRI tests showed promising results concerning the effect of using a dynamic brace. The brace showed a small visible spinal curve for both imaging techniques. The boneMRI results showed a lengthening of the spine between 4-7 mm in coronal plane, and between 3-5 mm in sagittal plane.

BoneMRI results show a time dependant effect on mechanical torsion due to forces acting on the spine. Immediately after applying loads, the total rotational value increased with 44°, while after one hour, the rotational values returned to their approximate starting value. Lengthening of the spine remained constant after one hour. During US testing the pressure inside the air cuffs changed over time, which could indicate a change in spinal alignment. It will be useful to repeat this test on a scoliotic patient for a longer period of time with a moderate scoliotic curve. The pressure inside the air cuffs did not change in supine position as the change in gravitational forces causes a smaller spinal curvature.

This study was a first step in the direction of creating a daily worn dynamic brace. The use of inflatable pressure regulated pads was validated and can be optimised further by increasing the number of pads while decreasing the size of them. Keeping the forces acting on the spine constant by changing the pressure inside the cuffs could improve the correctional effect and therefore the effectiveness of bracing. This effect is assumed to decrease for currently used braces because of the viscoelastic behaviour of the human body which needs to be tested on scoliotic patients for a larger period of time.

A method to improve brace effectiveness was developed, which can be tested more extensively on scoliotic patients using ultrasound. This can result in either advanced positioning and sizing of pressure pads for a static brace which needs to be altered over time (similar to the Ponseti method [43]), or a dynamic brace that alters the pressures automatically.

7

BIBLIOGRAPHY

[1] H. Labelle, C.-E. Aubin, R. Jackson, L. Lenke, P. Newton, and S. Parent, "Seeing the spine in 3D: how will it change what we do?," *J. Pediatr. Orthop.*, vol. 31, pp. S37–S45, 2011.

[2] P. Trobisch, O. Suess, and F. Schwab, "Idiopathic scoliosis," *Dtsch. Arztebl. Int.*, vol. 107, no. 49, p. 875, 2010.

[3] F. Altaf, A. Gibson, Z. Dannawi, and H. Noordeen, "Adolescent idiopathic scoliosis," *BMJ*, vol. 346, p. f2508, 2013.

[4] J. C. Cheng *et al.*, "Adolescent idiopathic scoliosis," *Nat Rev Dis Prim.*, vol. 1, p. 15030, 2015.

[5] A. Nachemson, "Report of the prevalence and natural history committee of the Scoliosis Research Society," in *the Annual Meeting of the Scoliosis Research Society; September 22, 1982; Denver, CO*, 1982.

[6] R. T. Morrissy, G. S. Goldsmith, E. C. Hall, D. Kehl, and G. H. Cowie, "Measurement of the Cobb angle on radiographs of patients who have," *J Bone Jt. Surg Am*, vol. 72, no. 3, pp. 320–327, 1990.

[7] S. L. Weinstein and I. V Ponseti, "Curve progression in idiopathic scoliosis.," *J. Bone Joint Surg. Am.*, vol. 65, no. 4, pp. 447–455, 1983.

[8] W. P. Bunnell, "The natural history of idiopathic scoliosis before skeletal maturity.," *Spine (Phila. Pa. 1976).*, vol. 11, no. 8, pp. 773–776, 1986.

[9] J. E. Lonstein and J. M. Carlson, "The prediction of curve progression in untreated idiopathic scoliosis," *J Bone Jt Surg*, pp. 1061–1071, 1984.

[10] E. Ascani *et al.*, "Natural history of untreated idiopathic scoliosis after skeletal maturity.," *Spine (Phila. Pa. 1976).*, vol. 11, no. 8, pp. 784–789, 1986.

[11] V. N. Cassar-Pullicino and S. M. Eisenstein, "Imaging in scoliosis: what, why and how?," *Clin. Radiol.*, vol. 57, no. 7, pp. 543–562, 2002.

[12] J. C. RISSER, "The iliac apophysis: an invaluable sign in the management of scoliosis," *Clin. Orthop. Relat. Res.*, vol. 11, pp. 111–119, 1958.

[13] H. Kim *et al.*, "Scoliosis imaging: what radiologists should know," *Radiographics*, vol. 30, no. 7, pp. 1823–1842, 2010.

[14] "<Brink - Consequences of the Three-Dimensional Pathoanatomy of Adolescent Idiopathic Scoliosis.pdf>."

[15] Stitzel, "7 Types of Scoliosis & Their Differences." [Online]. Available: https://www.treatingscoliosis.com/blog/scoliosis-types-differences/.

[16] "<Karimi - Scoliosis conservative treatment_ A review of literature.pdf>."

[17] S. L. Weinstein, L. A. Dolan, J. G. Wright, and M. B. Dobbs, "Effects of bracing in adolescents with idiopathic scoliosis," *N Engl J Med*, vol. 369, no. 16, pp. 1512–1521, 2013.

[18] S. L. Weinstein, L. A. Dolan, J. C. Y. Cheng, A. Danielsson, and J. A. Morcuende, "Adolescent idiopathic scoliosis," *Lancet*, vol. 371, no. 9623, pp. 1527–1537, 2008.

[19] N. Ramirez, C. E. I. I. Johnston, and R. H. Browne, "The prevalence of back pain in children who have idiopathic scoliosis," *JBJS*, vol. 79, no. 3, pp. 364–368, 1997.

[20] B. S. Richards, R. M. Bernstein, C. R. D'Amato, and G. H. Thompson, "<Richards - Standardization of Criteria for Adolescent Idiopathic Scoliosis brace studies.pdf>," *Spine*

(Phila. Pa. 1976)., vol. 30, no. 18, pp. 2068–2075, 2005.

[21]   R. S. Fayssoux, R. H. Cho, and M. J. Herman, "A history of bracing for idiopathic scoliosis in North America," *Clin Orthop Relat Res*, vol. 468, no. 3, pp. 654–664, 2010.

[22]   P. McAfee, "Bracing Treatment for Idiopathic Scoliosis," *Spine-Health*, 2002.

[23]   F. Canavese and A. Kaelin, "Adolescent idiopathic scoliosis: Indications and efficacy of nonoperative treatment," *Indian J. Orthop.*, vol. 45, no. 1, pp. 7–14, 2011.

[24]   G. T. Wynarsky and A. B. Schultz, "Optimization of skeletal configuration: studies of scoliosis correction biomechanics," *J. Biomech.*, vol. 24, no. 8, pp. 721–732, 1991.

[25]   M. D. Rigo, M. Villagrasa, and D. Gallo, "A specific scoliosis classification correlating with brace treatment: description and reliability," *Scoliosis*, vol. 5, no. 1, p. 1, Jan. 2010.

[26]   R. J. Fisk, J. E. Lonstein, and B. Malas, S, "<The Atlas of Spinal Orthotics.pdf>," *Orthot. Prosthetics*, 2017.

[27]   R. Pea, J. Dansereau, C. Caouette, N. Cobetto, and C. E. É. Aubin, "Computer-assisted design and finite element simulation of braces for the treatment of adolescent idiopathic scoliosis using a coronal plane radiograph and surface topography," *Clin Biomech (Bristol, Avon)*, vol. 54, no. July 2017, pp. 86–91, 2018.

[28]   W. Y. Chan *et al.*, "Mechanical and Clinical Evaluation of a Shape Memory Alloy and Conventional Struts in a Flexible Scoliotic Brace," *Ann Biomed Eng*, vol. 46, no. 8, pp. 1194–1205, 2018.

[29]   S. Negrini *et al.*, "Braces for idiopathic scoliosis in adolescents," *Spine (Phila. Pa. 1976).*, vol. 35, no. 13, pp. 1285–1293, 2010.

[30]   H.-R. R. Weiss, N. Tournavitis, X. Nan, M. Borysov, and L. Paul, "Workflow of CAD / CAM Scoliosis Brace Adjustment in Preparation Using 3D Printing," *Open Med Inf. J*, vol. 11, no. 1, pp. 44–51, 2017.

[31]   F. Bitonti, "<Bitonti - Micromechanical Assemblies and the Human Body.pdf>," *Archit. Des.*, vol. 87, no. 6, pp. 64–69, 2017.

[32]   J. Policy, "TREATING SCOLIOSIS WITH A 3D PRINTED TLSO," p. Stanford University College of Medicine.

[33]   N. Cobetto *et al.*, "Braces optimized with computer-assisted design and simulations are lighter, more comfortable, and more efficient than plaster-cast braces for the treatment of adolescent idiopathic scoliosis," *Spine Deform.*, vol. 2, no. 4, pp. 276–284, 2014.

[34]   J. I. Kessler, "Efficacy of a new computer-aided design/computer-aided manufacture orthosis in the treatment of adolescent idiopathic scoliosis," *J. Pediatr. Orthop. Part B*, vol. 17, no. 4, pp. 207–211, 2008.

[35]   R. C. Brink *et al.*, "A reliability and validity study for different coronal angles using ultrasound imaging in adolescent idiopathic scoliosis," *Spine J*, vol. 18, no. 6, pp. 979–985, 2018.

[36]   P. O. Newton, Y. Khandwala, C. E. Bartley, F. G. Reighard, T. P. Bastrom, and B. Yaszay, "New EOS imaging protocol allows a substantial reduction in radiation exposure for scoliosis patients," *Spine Deform.*, vol. 4, no. 2, pp. 138–144, 2016.

[37]   S. M. Presciutti, T. Karukanda, and M. Lee, "Management decisions for adolescent idiopathic scoliosis significantly affect patient radiation exposure," *Spine J.*, vol. 14, no. 9, pp. 1984–1990, 2014.

[38]   P. Knott *et al.*, "SOSORT 2012 consensus paper: reducing x-ray exposure in pediatric patients with scoliosis," *Scoliosis*, vol. 9, no. 1, p. 4, 2014.

[39]   A. Simony, E. J. Hansen, S. B. Christensen, L. Y. Carreon, and M. O. Andersen, "Incidence of cancer in adolescent idiopathic scoliosis patients treated 25 years previously," *Eur. Spine J.*, vol. 25, no. 10, pp. 3366–3370, 2016.

[40]   M. Li *et al.*, "Could clinical ultrasound improve the fitting of spinal orthosis for the patients with AIS?," *Eur. spine J.*, vol. 21, no. 10, pp. 1926–1935, 2012.

[41]   E. Lou *et al.*, "Brace wear characteristics during the first 6 months for the treatment of scoliosis," *Stud Heal. Technol Inf.*, vol. 176, pp. 346–349, 2012.

[42] F. Hefti, "Pathogenesis and biomechanics of adolescent idiopathic scoliosis (AIS)," *J. Child. Orthop.*, vol. 7, no. 1, pp. 17–24, 2013.

[43] R. B. Giesberts, E. E. G. Hekman, G. J. Verkerke, and P. G. M. Maathuis, "Rapid decrease of cast-induced forces during the treatment of clubfoot using the Ponseti method," *Bone Joint J.*, no. 100-B, pp. 1655–60, 2018.

[44] Sheri Amsel, "Vertebral Column Backbone) Labeling Page," *Exploring Nature Educational Resource*, 2019. [Online]. Available: http://www.exploringnature.org/db/view/3306.

[45] Boulder neurosurgical and spine associates, "Scoliosis & deformity." [Online]. Available: https://www.bnasurg.com/medical-conditions/scoliosis-deformity/.

[46] C. W. J. Cheung, G. Q. Zhou, S. Y. Law, T. M. Mak, K. L. Lai, and Y. P. Zheng, "Ultrasound Volume Projection Imaging for Assessment of Scoliosis," *IEEE Trans Med Imaging*, vol. 34, no. 8, pp. 1760–1768, 2015.

[47] M. S. Wong, A. F. T. Mak, K. D. K. Luk, J. H. Evans, and B. Brown, "Effectiveness and biomechanics of spinal orthoses in the treatment of adolescent idiopathic scoliosis (AIS)," *Prosthet. Orthot. Int.*, vol. 24, no. 2, pp. 148–162, 2000.

[48] E. Chalmers, E. Lou, D. Hill, V. H. Zhao, and M.-S. Wong, "Development of a pressure control system for brace treatment of scoliosis," *IEEE Trans. Neural Syst. Rehabil. Eng.*, vol. 20, no. 4, pp. 557–563, 2012.

[49] E. Lou, D. L. Hill, J. V Raso, M. J. Moreau, and J. K. Mahood, "Smart orthosis for the treatment of adolescent idiopathic scoliosis," *Med. Biol. Eng. Comput.*, vol. 43, no. 6, pp. 746–750, 2005.

[50] H. Jiang, "Interface pressure in the Boston brace treatment of scoliosis. A preliminary study," in *International Symposium on 3D Scoliotic Deformities*, 1992.

[51] D. Perie, C. E. Aubin, Y. Petit, M. Beausejour, J. Dansereau, and H. Labelle, "Boston brace correction in idiopathic scoliosis: a biomechanical study," *Spine (Phila Pa 1976)*, vol. 28, no. 15, pp. 1672–1677, 2003.

[52] T. P. C. Schlösser *et al.*, "Three-dimensional characterization of torsion and asymmetry of the intervertebral discs versus vertebral bodies in adolescent idiopathic scoliosis," *Spine (Phila. Pa. 1976).*, vol. 39, no. 19, pp. E1159–E1166, 2014.

[53] S.-A. Scherrer, M. Begon, A. Leardini, C. Coillard, C.-H. Rivard, and P. Allard, "Three-dimensional vertebral wedging in mild and moderate adolescent idiopathic scoliosis," *PLoS One*, vol. 8, no. 8, pp. e71504–e71504, Aug. 2013.

[54] C. L. Chung *et al.*, "Mechanical Testing of a Novel Fastening Device to Improve Scoliosis Bracing Biomechanics for Treating Adolescent Idiopathic Scoliosis," *Appl. bionics Biomech.*, vol. 2018, 2018.

[55] C. He *et al.*, "An effective assessment method of spinal flexibility to predict the initial in-orthosis correction on the patients with adolescent idiopathic scoliosis (AIS)," *PLoS One*, vol. 12, no. 12, p. e0190141, 2017.

[56] R. C. Brink *et al.*, "Upright, prone, and supine spinal morphology and alignment in adolescent idiopathic scoliosis," *Scoliosis spinal Disord.*, vol. 12, no. 1, p. 6, 2017.

[57] M. Lee, G. P. Steven, J. Crosbie, and R. Higgs, "Towards a theory of lumbar mobilisation–the relationship between applied manual force and movements of the spine," *Man. Ther.*, vol. 1, no. 2, pp. 67–75, 1996.

[58] M. K. Barnett, "A brief history of thermometry," *J. Chem. Educ.*, vol. 18, no. 8, p. 358, 1941.

[59] R. Zheng *et al.*, "Factors influencing spinal curvature measurements on ultrasound images for children with adolescent idiopathic scoliosis (AIS)," *PLoS One*, vol. 13, no. 6, pp. e0198792–e0198792, Jun. 2018.

8
APPENDIX
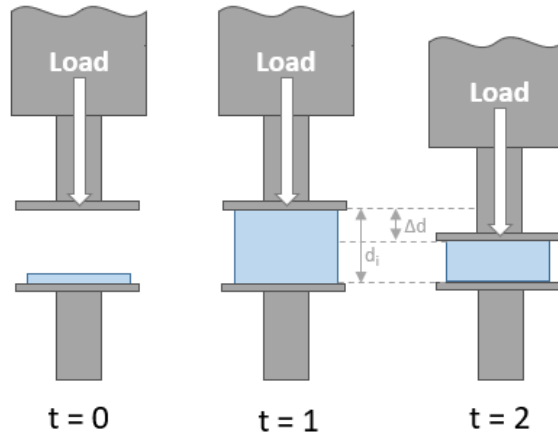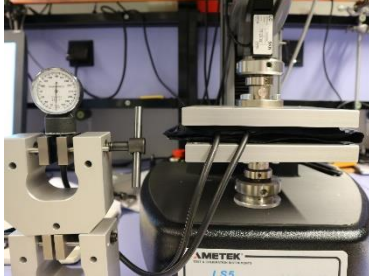
APPENDIX I
Overview of brace concepts

	Vacuum forming			Prefabricated		3D printing
	Plaster cast	CAD/CAM	CAD/CAM + FEM	Rigid brace	Soft brace	
	Wilmington brace [26]	Lyon ART brace [26]	Research trial brace [33]	Boston brace module [21]	SpinceCor brace [21]	UNYQ brace [31]
+	Efective Patient specific	Effective Patient specific Reproducible Accurate	Effective Patient specific Reproducible Accurate Light weight Low body surface coverage	Effective Fast availability Easy to modify	Fast availability Easy to modify High comfort	Patient specific Reproducibility Aesthetical Thickness variability Light weight Aeration
-	Low reproducibility No future reference data Material waste Low accuracy Unpleasant for patient Long fabrication time	High investment costs Long learning curve Material waste	High investment costs Long learning curve Material waste Extra X-Ray Based on assumptions Complex	Not patient specific Does not fit everyone Needs service	Not patient specific Questionable effectiveness Loosening after time For low Cobb angles only Difficulty of toiletting	High investments costs Long learning curve No tool available to easily adapt CAD file

APPENDIX II

Compression test setups

Setup A
1. d_i = 20 mm
2. d_i = 30 mm
3. d_i = 40 mm

Setup B
4. d_i = infinite
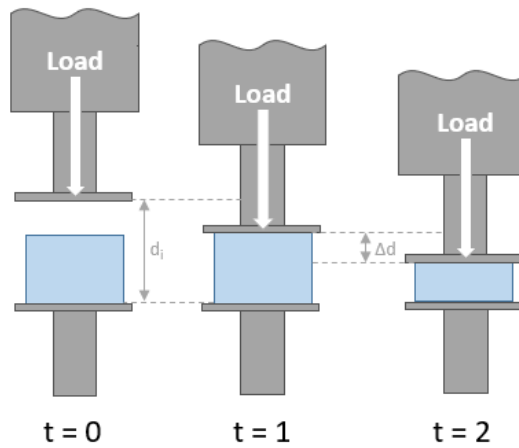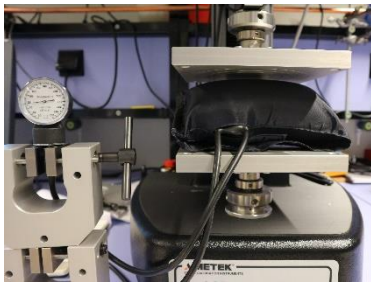
Setup C
5. d_i = infinite

50
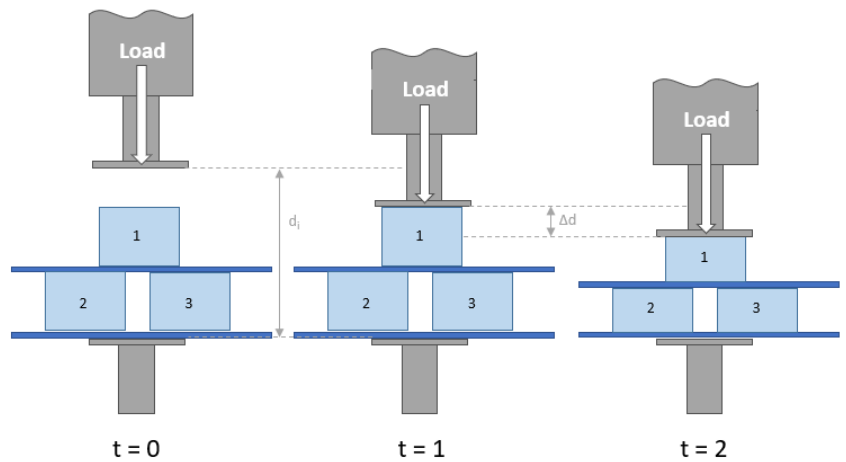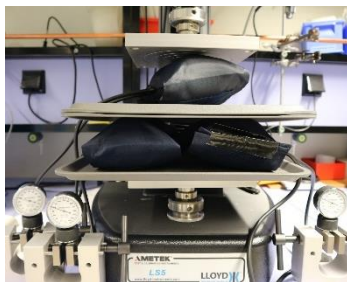
APPENDIX III
Executed Ultrasound tests

	Sequence	Pressure [mmHg]	Amount of repetitions	Time [min]
Test A	1	0	0	t=0
	2	100	0	t=0
	3	150	0	t=0
	4	200	0	t=0
Test B	1	0	1	t=0
	2	100	1	t=0
	3	100	1	t=60
	4	100	1	t=120
Test C	1	0	1	t=0
	2	200	1	t=0
	3	200	1	t=60
	4	200	1	t=120

Stress relaxation measurements

Setup B
Initial displacement: infinite

Setup C
Initial displacement: infinite
Initial pressure: 100 mmHg
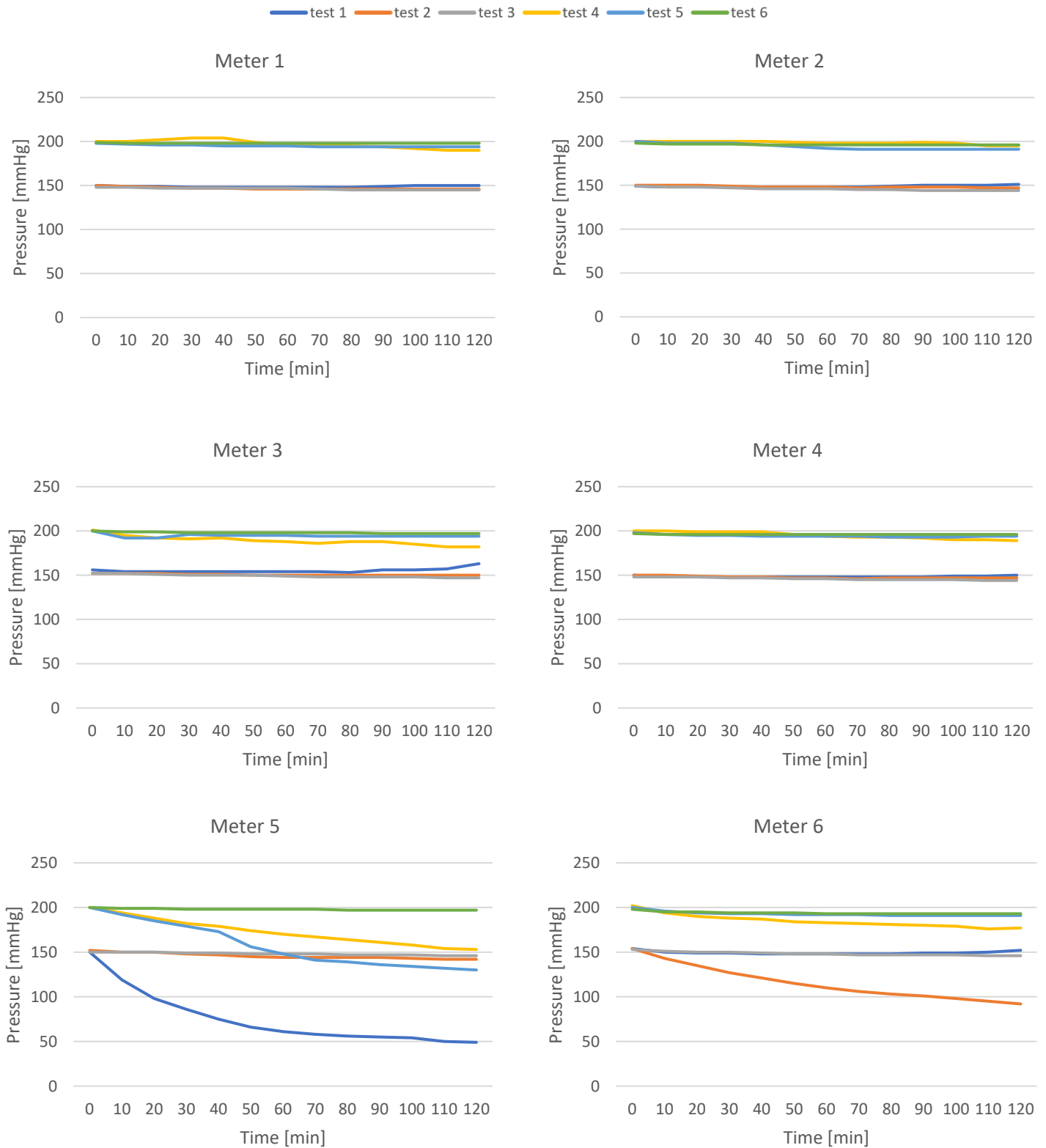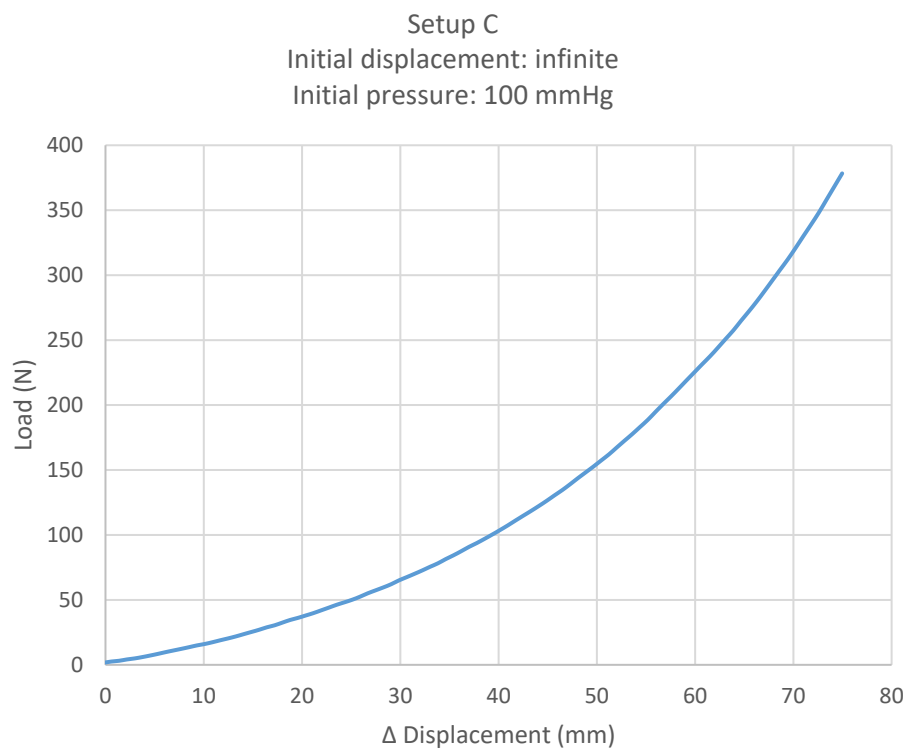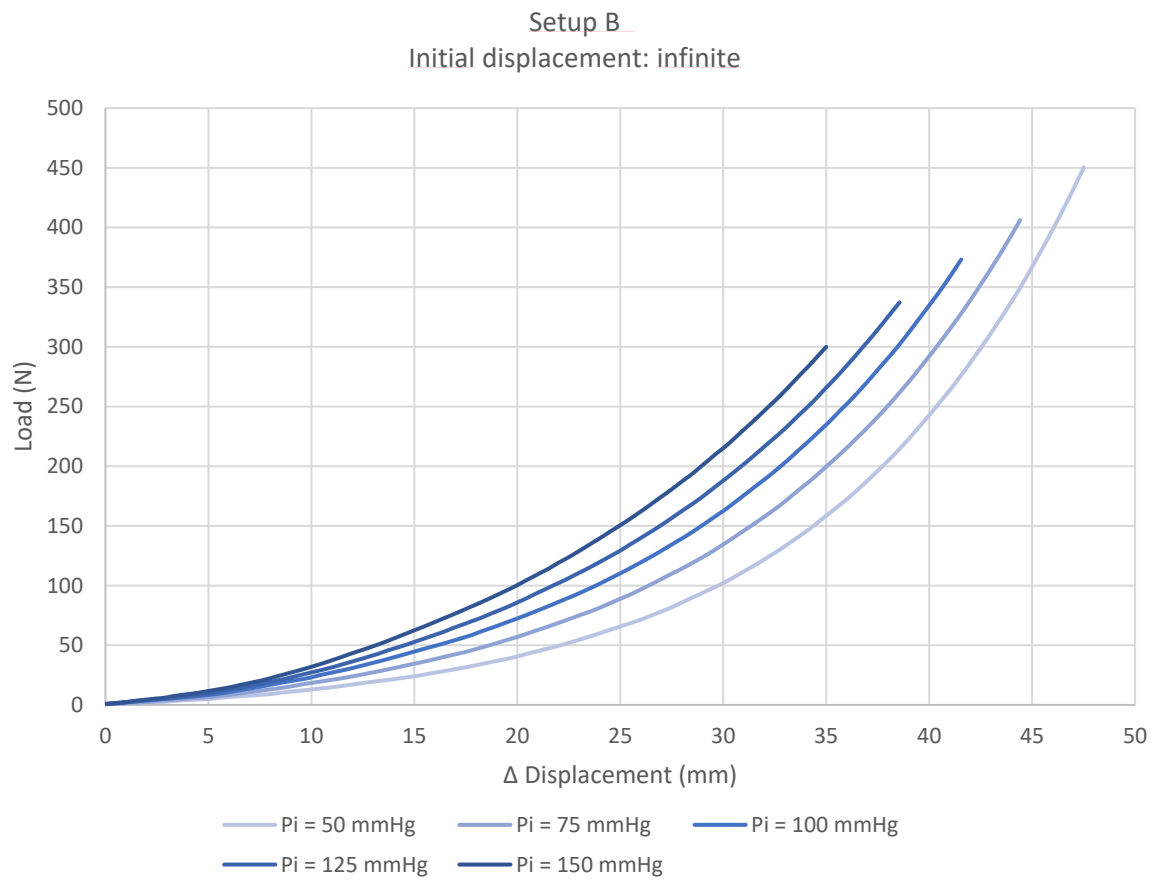
Internal pressure equations

$$L_{P=50}(d) = -4.1 \cdot d + 197$$
$$L_{P=75}(d) = -5.5 \cdot d + 292$$
$$L_{P=100}(d) = -6.5 \cdot d + 372$$
$$L_{P=125}(d) = -7.4 \cdot d + 451$$
$$L_{P=150}(d) = -8.2 \cdot d + 533$$
$$L_{P=175}(d) = -8.7 \cdot d + 608$$
$$L_{P=200}(d) = -9.8 \cdot d + 372$$
$$L_{P=225}(d) = -10.9 \cdot d + 790$$
$$L_{P=250}(d) = -11.6 \cdot d + 867$$

APPENDIX VII
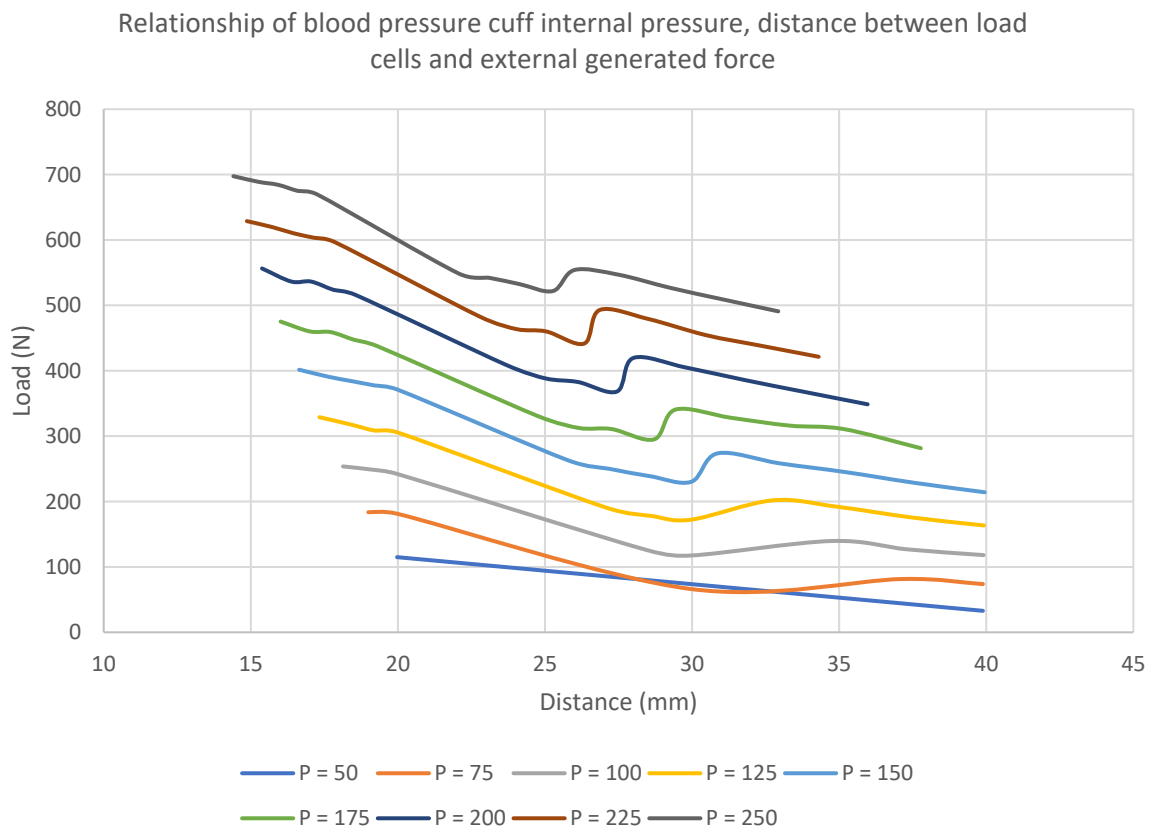
Figure VI: All lines indicate the blood pressure cuff internal pressures for a specific distance between the load cells. These are the combined results of the three compression tests.

Internal pressure standing position
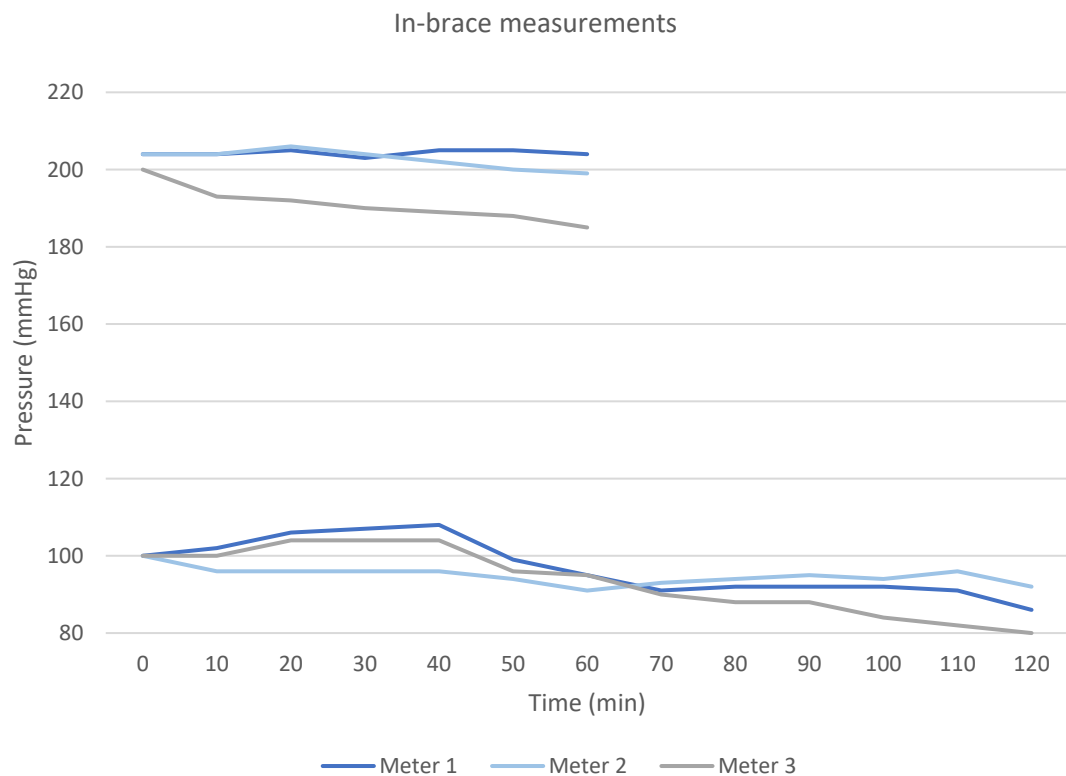
Figure VIII.: Internal pressure values of the blood pressure cuffs when wearing the brace. There was no air released or added during the experiment. The experiment was executed two times, once with initial pressures of 200 mmHg and once with initial pressures of 100 mmHg. The experiment with initial pressures of 200 mmHg lasted for 60 minutes as this experiment was ceased early.
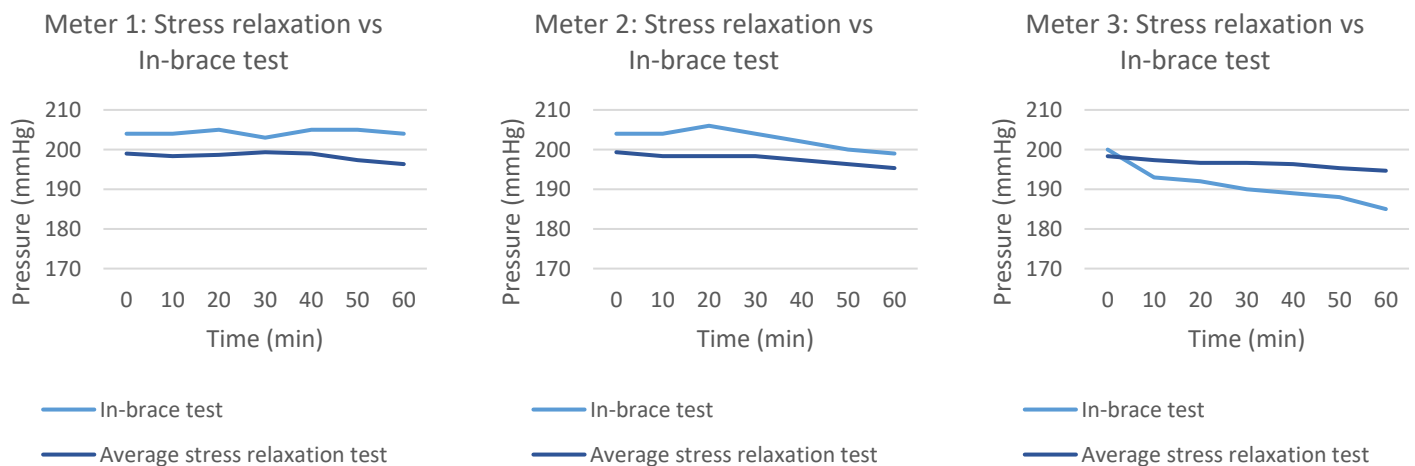
Internal pressure in-brace versus stress relaxation test

Figure IX: Comparison of pressure values while wearing the brace and during the stress relaxation test. Every graph shows the results per meter. Meter 1 is positioned on the upper left side of the body, meter 2 on the lower left side and meter 3 is the single cuff on the right side.

APPENDIX X

Internal pressure supine position

Internal pressure changes while laying down
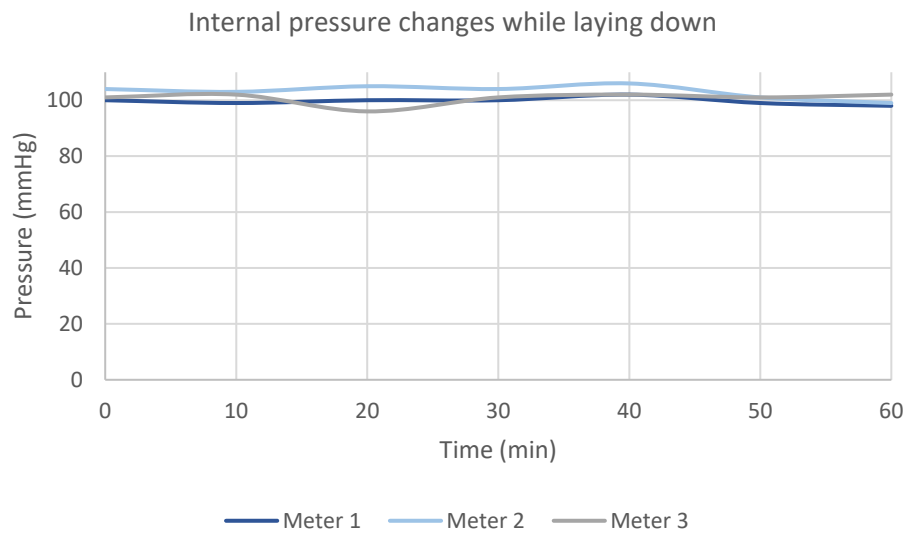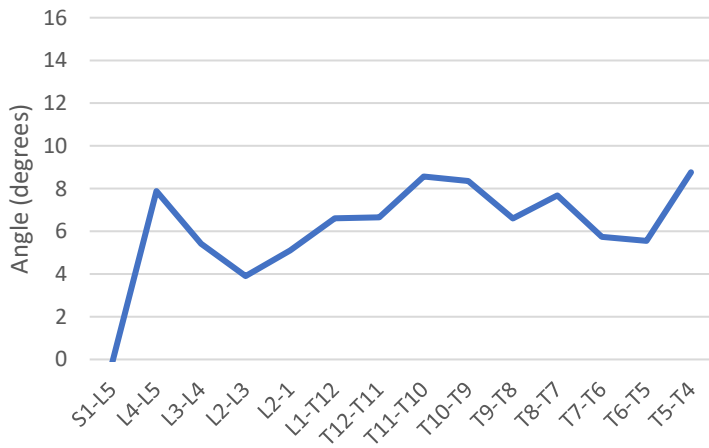
Pressure (mmHg) vs Time (min)

Figure X: Internal pressure values for all three blood pressure cuffs. The values were documented every ten minutes.
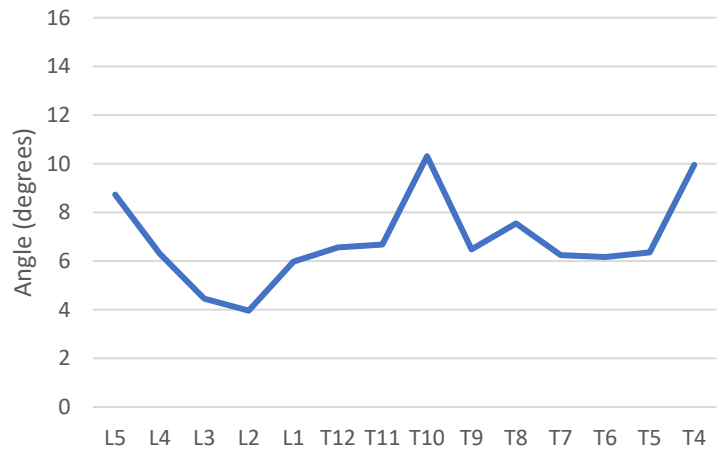
APPENDIX XI
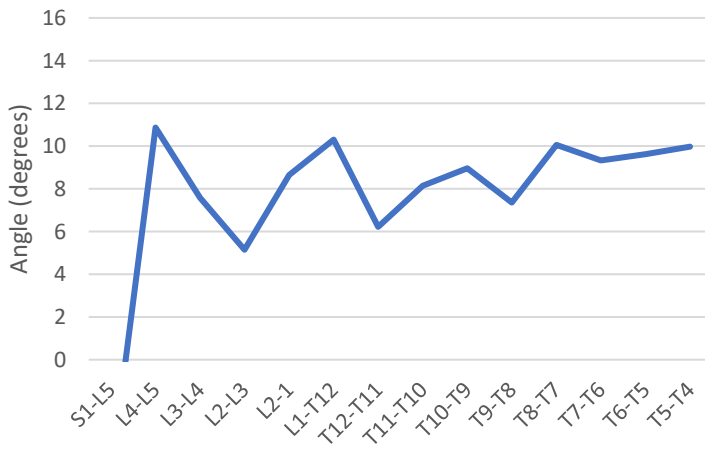Mechanical torsion visualized per disc and vertebrae.
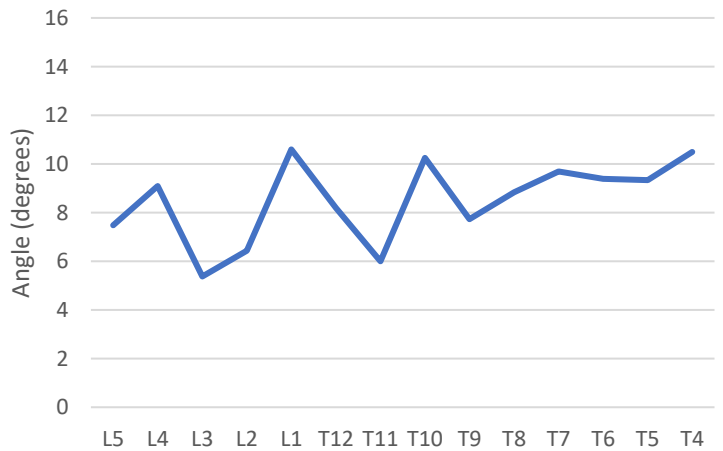

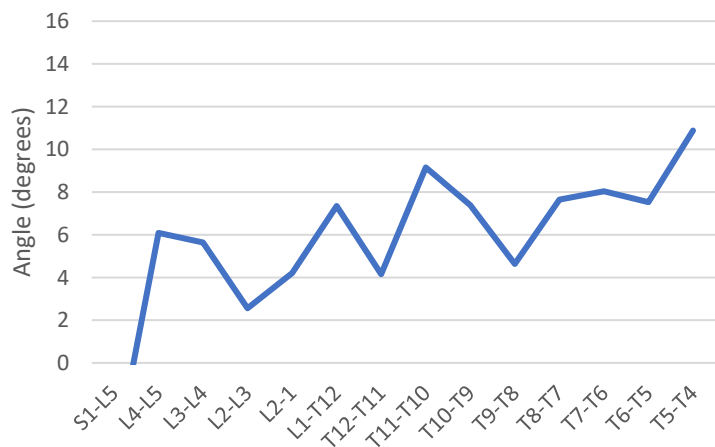Disc rotation
P=0
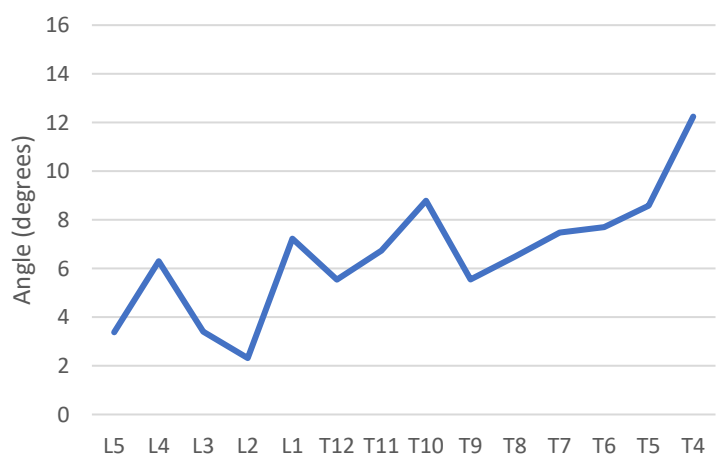
Vertebral rotation
P=0

Disc rotation
P=100, t=0

Vertebral rotation
P=100, t=0

Disc rotation
P=100, t=60

Vertebral rotation
P=100, t=60

APPENDIX XII

Measurements of apical regions.

Apical region T6, includes the adjacent segments below and above. In this case the vertebrae T7 until T5 are included.

	Total length left	Total length right	Disc length left	Disc length right	Vertebral length left	Vertebral length right
P=0	59	59	11	12	47	47
P=100 t=0	59	61	9,9	11	49	50
P=100 t=60	58	61	12	13	47	48

Apical region T12, includes the adjacent segments below and above. In this case the vertebrae L1 until T11 are included.

	Total length left	Total length right	Disc length left	Disc length right	Vertebral length left	Vertebral length right
P=0	80	81	15	16	65	66
P=100 t=0	81	80	16	15	65	65
P=100 t=60	82	81	16	17	66	64